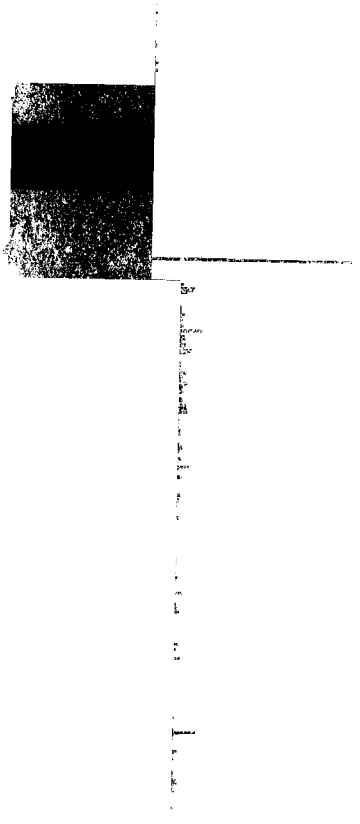

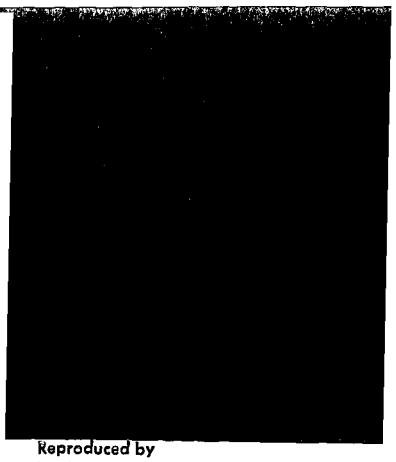

BELLCOMM, INC.
955 L'ENFANT PLAZA NORTH, S.W. WASHINGTON, D.C. 20024

COVER SHEET FOR TECHNICAL MEMORANDUM

TITLE- Equilibrium Properties of the Skylab CMG Rotation Law

TM- 72-1022-2

DATE- March 31, 1972

FILING CASE NO(S)- 620

AUTHOR(S)- B. D. Elrod
G. M. Anderson

FILING SUBJECT(S)- (ASSIGNED BY AUTHOR(S)- Control Moment Gyros, Spacecraft Attitude Control, Skylab Program

ABSTRACT

The rotation law is intended to produce gimbal rates ($\underline{\dot{\delta}}$) which distribute the angular momentum contributions among the CMGs to avoid gimbal stop encounters. This investigation was undertaken to develop an understanding of its implications for gimbal angle management under various angular momentum situations. Conditions were obtained for the existence of equilibria (gimbal angles, $\underline{\delta}_E$, for $\underline{\dot{\delta}}=0$) and corresponding stability properties. It was shown that $\underline{\delta}_E$ is either asymptotically stable or unstable in a region about $\underline{\delta}_E$.

Plots of asymptotically stable $\underline{\delta}_E$ for constant momentum direction ($\underline{h}$) define equilibrium-loci which the CMGs tend to follow in gimbal angle space as momentum magnitude (H) varies. Multiple $\underline{\delta}_E$ loci were shown to exist for both 2 and 3 CMGs with some "undesirable" loci extending to the gimbal stops. At H=0 the origin $\underline{\delta}_E$ was observed to be a unique asymptotically stable equilibrium for 3, but not 2 CMGs. Consequently 3 CMGs have a natural recovery capability (to $\underline{\delta}_E=\underline{0}$) as H→0 whereas 2 CMGs do not and in fact, multiple $\underline{\delta}_E$ commonly occur near H=0. Normal caging operations with 2 CMGs can lead to acquiring an undesirable $\underline{\delta}_E$ locus and a subsequent gimbal stop encounter.

A simple modification that increases the rotation law's flexibility was developed based on the concept of a dynamic origin. With this approach avoidance of undesirable $\underline{\delta}_E$ loci from caging operations was demonstrated for 2 CMGs.

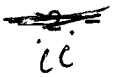

The present rotation law implementation includes limiting of certain variable parameters, ostensibly for control of transient response. Depending on momentum conditions this can increase the number of multiple $\underline{\delta}_E$ and the potential of a gimbal stop encounter regardless of initial gimbal angles. This was illustrated by an example for 2 CMGs. An alternate limiting arrangement was suggested that does not affect equilibrium properties.

Table of Contents

~~2~~
IV

Bellcomm
955 L'Enfant Plaza North, S.W.
Washington, D. C. 20024

date:

to: Distribution

TM-72-1022-2

from: B. D. Elrod, G. M. Anderson

subject: Equilibrium Properties of the Skylab CMG Rotation Law - Case 620

TECHNICAL MEMORANDUM

1.0 Introduction

The Skylab Control Moment Gyro (CMG) control law is divided into two parts, i.e.

The steering law, and

The rotation law

The role of the steering law is to allocate the desired change in angular momentum among the participating CMGs and thereby develop the desired control torque on the vehicle. The rotation law is intended to redistribute the angular momentum among the CMG's in such a way as to minimize gimbal stop encounters. The rotation law conserves system angular momentum and therefore does not produce any torque on the vehicle.

Gimbal angle limits were introduced into the CMG development to avoid the mechanical and electrical problems of slip rings and brushes. That decision eased the hardware development but complicated the software design.

It is apparent that gimbal stop encounters should be minimized. The system is in danger of loss of control with a gimbal in contact with a stop. The Skylab design provides alternative means for recovery from this condition although it could be expensive, in terms of consumable propellants. The preferable course is to avoid, or at least to minimize, gimbal stop encounters. The rotation law is the chosen instrument for this purpose.

Perhaps the main feature of the rotation law is that it is an equilibrium process. Secondly, since the usual torque demands are slowly varying compared to CMG gimbal angle rate capability, it is likely to find the system in the vicinity of its equilibrium.

These two attributes raise the possibility of developing a model for understanding and predicting CMG behavior under a wide class of conditions. What is required is a knowledge of the equilibrium process involved, and particularly of the location of the points of equilibrium. Since the equilibria are independent of CMG dynamics, they have a permanent value and once determined can be compiled for future use and reference.

There is a further point. We have found that multiple equilibria exist. These multiple points exist even for simply connected regions of acceptable gimbal angles, i.e. regions not separated by gimbal limits and in which the angular momentum constraint is satisfied. In some cases there are preferable points of equilibrium. A preferred point is one in which the future motion of the point is well behaved as opposed to an alternate point that may subsequently encounter a gimbal stop. The implications for CMG management of these considerations appears to be substantial.

This memorandum treats the following topics:

Equilibrium Process

Allowable Gimbal Angle Space

Evaluation of Equilibria and Possible Problem Areas

Possible Rotation Law Modification

Suggested Areas for Further Research

Summary and Conclusion

A word is in order on the scope of the treatment. The ideas developed and presented here had their beginnings nearly a year ago at the time Kranton and Chu were running digital simulations of Kranton's and the Skylab control law.[6] Often the gimbal angles would exhibit rapid transients without apparent explanation. At that time the investigators were restricted to changing constants and rerunning the problem in the search for improved response. No method was available to guide this search.

Also, at the same time, D. A. DeGraaf had uncovered some evidence of multiple equilibria. This naturally raised the question of how many equilibria, at constant angular momentum, actually exist.

With the press of other matters we were not able to move this project as rapidly as we had wished. It was late September before some of the major theoretical hurdles were overcome. However, by then we were running out of time. We no longer had the possibility to exhaust the equilibrium subject, for example, by computing a wide range of cases and then publishing the results.

What we have chosen to do, since an encyclopedic treatment is foreclosed, is to present the theoretical results and to amplify them with some illustrative examples. This method will show what we believe to be the power of this approach and its potential utility for gimbal angle management of Skylab CMGs. It will remain for others to carry these results forward for practical use if that is deemed worthy of pursuing.

2.0 The Equilibrium Process

It was asserted above that the rotation law is an equilibrium process. Some of the significant attributes, or properties, of the control system stemming from this observation have already been suggested. These are developed more fully later on. Before that, it is necessary to prove the assertion regarding equilibrium.

Necessary and sufficient conditions are derived here for equilibrium. Because of the length of the proof, the necessary conditions are removed to Appendix A. Stability is treated subsequently, and conditions for either asymptotic stability or instability of the equilibria are established.

This section also includes the determination of a performance function of gimbal angles minimized by the rotation law.

In this treatment we shall not repeat the derivation of the rotation law. Interested readers are referred to the PDD[1] or for a good exposition, to Kranton[2].

We retain here much of Kranton's matrix formulation for the economies of presentation that it offers. The connection with PDD notation is given at critical junctures.

The gimbal angles are defined as follows:

$$(1) \qquad \underline{\delta} = \begin{Bmatrix} \delta_1 \\ \delta_2 \\ \delta_3 \\ \delta_4 \\ \delta_5 \\ \delta_6 \end{Bmatrix} = \begin{Bmatrix} \delta_{1(1)} \\ \delta_{3(1)} - 45° \\ \delta_{1(2)} \\ \delta_{3(2)} - 45° \\ \delta_{1(3)} \\ \delta_{3(3)} - 45° \end{Bmatrix} \equiv \begin{Bmatrix} \hat{\delta}_1 \\ \hat{\delta}_2 \; -45° \\ \hat{\delta}_3 \\ \hat{\delta}_4 \; -45° \\ \hat{\delta}_5 \\ \hat{\delta}_6 \; -45° \end{Bmatrix}$$

where the vector in the middle is in PDD notation. (See Fig. 1)

The relationships between gimbal angle rates and the angular rotation rates ($\underline{\omega}_1$, $\underline{\omega}_2$, $\underline{\omega}_3$) of the CMG angular momenta are, following Kranton[2],*

$$(2) \qquad \dot{\underline{\delta}}_1 = \begin{Bmatrix} \dot{\delta}_1 \\ \dot{\delta}_2 \end{Bmatrix} = R_1 \underline{\omega}_1 \qquad \text{CMG 1}$$

$$(3) \qquad \dot{\underline{\delta}}_2 = \begin{Bmatrix} \dot{\delta}_3 \\ \dot{\delta}_4 \end{Bmatrix} = R_2 \underline{\omega}_2 \qquad \text{CMG 2}$$

$$(4) \qquad \dot{\underline{\delta}}_3 = \begin{Bmatrix} \dot{\delta}_5 \\ \dot{\delta}_6 \end{Bmatrix} = R_3 \underline{\omega}_3 \qquad \text{CMG 3}$$

where

$$(5) \qquad R_1 = \begin{bmatrix} s\hat{\delta}_2 & c\hat{\delta}_2 & 0 \\ -t\hat{\delta}_1 c\hat{\delta}_2 & t\hat{\delta}_1 s\hat{\delta}_2 & -1 \end{bmatrix}$$

---

*Abbreviations s,c, and t are used respectively for the sin, cos and tan functions. The superscript T on a vector or matrix denotes the transpose operation.

(6) $$R_2 = \begin{bmatrix} 0 & s\hat{\delta}_4 & c\hat{\delta}_4 \\ -1 & -t\hat{\delta}_3 c\hat{\delta}_4 & t\hat{\delta}_3 s\hat{\delta}_4 \end{bmatrix}$$

(7) $$R_3 = \begin{bmatrix} c\hat{\delta}_6 & 0 & s\hat{\delta}_6 \\ t\hat{\delta}_5 s\hat{\delta}_6 & -1 & -t\hat{\delta}_5 c\hat{\delta}_6 \end{bmatrix}$$

The rotation law is given by

(8) $$\underline{\delta} = D\underline{\lambda}$$

where*

(9) $$\underline{\lambda} = -K_R\, D^T Q \underline{\delta} = \begin{pmatrix} \varepsilon_{RA} \\ \varepsilon_{RB} \\ \varepsilon_{RC} \end{pmatrix}$$

(10) $$D = \begin{bmatrix} R_1\underline{h}_2 & \underline{0} & R_1\underline{h}_3 \\ R_2\underline{h}_1 & R_2\underline{h}_3 & \underline{0} \\ \underline{0} & R_3\underline{h}_2 & R_3\underline{h}_1 \end{bmatrix} = \begin{bmatrix} \begin{pmatrix} S_{A11} \\ S_{A31} \end{pmatrix} & \begin{pmatrix} 0 \\ 0 \end{pmatrix} & \begin{pmatrix} S_{C11} \\ S_{C31} \end{pmatrix} \\ \begin{pmatrix} S_{A12} \\ S_{A32} \end{pmatrix} & \begin{pmatrix} S_{B12} \\ S_{B32} \end{pmatrix} & \begin{pmatrix} 0 \\ 0 \end{pmatrix} \\ \begin{pmatrix} 0 \\ 0 \end{pmatrix} & \begin{pmatrix} S_{B13} \\ S_{B33} \end{pmatrix} & \begin{pmatrix} S_{C13} \\ S_{C33} \end{pmatrix} \end{bmatrix}$$

and

---

*$(\varepsilon_{RA}, \varepsilon_{RB}, \varepsilon_{RC})$ represent the PDD notation.

(11) $$Q = \begin{bmatrix} 1 & & \\ .457 & 1 & \\ & .457 & 1 \\ & & .457 \end{bmatrix}$$

The matrix on the right in Eq. (10) is in PDD notation. The symbols $\underline{h}_1$, $\underline{h}_2$ and $\underline{h}_3$ are unit vectors coincident with the CMG angular momentum vectors. The symbol K_R is a constant that can be adjusted to vary the dynamics of the rotation law.

In the current rotation law design individual elements of D^T in Eq. (9) are limited in magnitude to a constant SL (currently SL=.04).[1] That in effect introduces additional non-linearity into the control system without any theoretical foundation as to its potential effect on gimbal stop avoidance. We confine our attention initially to the case with no limiting and later compare some of our results to the case with limiting.

2.1 Conditions for Equilibrium

The equilibrium condition is one that results in

(12) $$\dot{\underline{\delta}} = \underline{0}$$

The necessary and sufficient condition for equilibrium is

(13) $$\underline{\lambda} = \underline{0}$$

That Eq. (13) is a sufficient condition for equilibrium is evident from Eq. (8). A proof that Eq. (13) is necessary as well, is given in Appendix A. Another formulation of the rotation law dynamics which leads directly to Eq. (13) as the equilibrium condition is developed in Section 2.3 for the stability analysis.

2.2 A Performance Function of Gimbal Angles

Since the rotation law is a conservative process, i.e. there is no torque interaction with the spacecraft, it is natural to expect that the associated dynamics should be derivable from a potential or, as used here, performance function.* Equilibria of the system would then correspond to extrema of the performance function.

As our current interest is in the equilibria themselves, in order to simplify the analysis, we exclude the system dynamics from consideration and inquire into the existence of a performance function whose extrema correspond with the system equilibria.** It was anticipated that the availability of such a function would be of value in locating the points of equilibrium. That expectation was realized. This method is perhaps the best available for systematic study of the equilibria for two CMGs and is a useful aid for the three CMG case.

Let

$$P = P(\delta_1, \delta_2, \ldots \delta_6) = P(\underline{\delta}) \tag{14}$$

designate the desired function of gimbal angles. The free, or independent, variables are the rotations

$$\phi_{12} \text{ about } \underline{h}_{12} = \underline{h}_1 + \underline{h}_2$$
$$\phi_{23} \text{ about } \underline{h}_{23} = \underline{h}_2 + \underline{h}_3$$
$$\phi_{31} \text{ about } \underline{h}_{31} = \underline{h}_3 + \underline{h}_1$$

---

*We prefer the performance designation since we are concerned with a measure of rotation law effectiveness.

**More exactly, we limit the applicability of the performance function to a small region about an equilibrium. In this region the system dynamics are related to the performance function and it is possible therefore to treat stability using this function. We suspect that it is possible to derive the entire CMG dynamics using a Lagrangian formulation in which the potential function would play the role of what is here termed the performance function. Time has not permitted the exploration of this idea.

The rotation rate vector, $\underline{\omega}_{12}$, is related to ϕ_{12} by

$$\underline{\omega}_{12} = \frac{d\phi_{12}}{dt} \frac{(\underline{h}_1+\underline{h}_2)}{|\underline{h}_1+\underline{h}_2|} = \frac{(\underline{h}_1+\underline{h}_2)}{H_{12}} \dot{\phi}_{12} \tag{15}$$

From Eqs. (2) and (3) and the fact that $R_i\underline{h}_i=\underline{0}$* it follows that

$$\begin{pmatrix} \partial\delta_1/\delta t \\ \partial\delta_2/\delta t \end{pmatrix} = R_1\underline{\omega}_{12} = \frac{R_1\underline{h}_2}{H_{12}} \dot{\phi}_{12}$$

$$\begin{pmatrix} \partial\delta_3/\delta t \\ \partial\delta_4/\delta t \end{pmatrix} = R_2\underline{\omega}_{12} = \frac{R_2\underline{h}_1}{H_{12}} \dot{\phi}_{12}$$

and, therefore,

$$\begin{pmatrix} \partial\delta_1/\partial\phi_{12} \\ \partial\delta_2/\delta\phi_{12} \end{pmatrix} = \frac{1}{H_{12}} \begin{pmatrix} (R_1\underline{h}_2)_1 \\ (R_1h_2)_2 \end{pmatrix} = \frac{R_1\underline{h}_2}{H_{12}} \tag{16}$$

$$\begin{pmatrix} \partial\delta_3/\partial\phi_{12} \\ \partial\delta_4/\partial\phi_{12} \end{pmatrix} = \frac{1}{H_{12}} \begin{pmatrix} (R_2\underline{h}_1)_1 \\ (R_2\underline{h}_1)_2 \end{pmatrix} = \frac{R_2\underline{h}_1}{H_{12}} \tag{17}$$

By definition of the pairwise rotation ϕ_{12} we note that

$$\begin{pmatrix} \partial\delta_5/\partial\phi_{12} \\ \partial\delta_6/\partial\phi_{12} \end{pmatrix} = \begin{pmatrix} 0 \\ 0 \end{pmatrix} \tag{18}$$

We use the fact that the system equilibria are governed by the condition $\lambda = 0$ to determine a performance function in accord with our limited objectives. Accordingly, as the defining relation, we take

---

*See Eqs. (5)-(7) and Eq. (B-1) of Appendix B.

$$(19) \qquad \frac{\partial P}{\partial \underline{\phi}} = \begin{Bmatrix} \partial P/\partial \phi_{12} \\ \partial P/\partial \phi_{23} \\ \partial P/\partial \phi_{31} \end{Bmatrix} \equiv -\frac{1}{K_R} H^{-1} \underline{\lambda}$$

where

$$(20) \qquad H \equiv \begin{bmatrix} |\underline{h}_1+\underline{h}_2| & 0 & 0 \\ 0 & |\underline{h}_2+\underline{h}_3| & 0 \\ 0 & 0 & |\underline{h}_3+\underline{h}_1| \end{bmatrix} = \begin{bmatrix} H_{12} & \bigcirc & \\ \bigcirc & H_{23} & \\ & & H_{31} \end{bmatrix}$$

Using Eqs. (9), (10) and (16)-(18) we can write $\partial P/\partial \phi_{12}$ as

$$(21) \qquad \frac{\partial P}{\partial \phi_{12}} = \delta_1 \frac{\partial \delta_1}{\partial \phi_{12}} + q\delta_2 \frac{\partial \delta_2}{\partial \phi_{12}} + \delta_3 \frac{\partial \delta_3}{\partial \phi_{12}} + q\delta_4 \frac{\partial \delta_4}{\partial \phi_{12}} + \delta_5 \frac{\partial \delta_5}{\partial \phi_{12}} + q\delta_6 \frac{\partial \delta_6}{\partial \phi_{12}}$$

$$= (\partial \underline{\delta}/\partial \phi_{12})^T Q \underline{\delta}$$

where $q = 0.457$ for the present Skylab design. Similar treatment for $\partial P/\partial \phi_{23}$ and $\partial P/\partial \phi_{31}$ leads to

$$(22) \qquad \frac{\partial P}{\partial \underline{\phi}} = \begin{Bmatrix} \partial \underline{\delta}/\partial \phi_{12} \\ \partial \underline{\delta}/\partial \phi_{23} \\ \partial \underline{\delta}/\partial \phi_{31} \end{Bmatrix}^T Q \underline{\delta} = \frac{\partial}{\partial \underline{\phi}} \left(\frac{1}{2} \underline{\delta}^T Q \underline{\delta}\right)$$

Thus P for the Skylab CMG rotation law is a quadratic function of gimbal angles

$$(23) \qquad P(\underline{\delta}) = \frac{1}{2} \underline{\delta}^T Q \underline{\delta}$$

with extrema occurring whenever $\underline{\lambda} = 0$.

2.3 Stability Analysis

With the performance function and the condition for equilibrium established it remains to examine stability of the equilibria. This will be based on an equivalent formulation of the rotation law dynamics in terms of $\dot{\underline{\phi}} = (\dot{\phi}_{12}, \dot{\phi}_{23}, \dot{\phi}_{31})^T$ rather than the gimbal rates $\dot{\underline{\delta}}$ as in Eq. (8). The relationship between $\dot{\underline{\delta}}$ and $\dot{\underline{\phi}}$ is

$$\dot{\underline{\delta}} = \begin{Bmatrix} \dot{\underline{\delta}}_1 \\ \dot{\underline{\delta}}_2 \\ \dot{\underline{\delta}}_3 \end{Bmatrix} = \begin{bmatrix} \partial\underline{\delta}_1/\partial\phi_{12} & \partial\underline{\delta}_1/\partial\phi_{23} & \partial\underline{\delta}_1/\partial\phi_{31} \\ \partial\underline{\delta}_2/\partial\phi_{12} & \partial\underline{\delta}_2/\partial\phi_{23} & \partial\underline{\delta}_2/\partial\phi_{31} \\ \partial\underline{\delta}_3/\partial\phi_{12} & \partial\underline{\delta}_3/\partial\phi_{23} & \partial\underline{\delta}_3/\partial\phi_{31} \end{bmatrix} \begin{Bmatrix} \dot{\phi}_{12} \\ \dot{\phi}_{23} \\ \dot{\phi}_{31} \end{Bmatrix}$$

$$= \begin{bmatrix} R_1\underline{h}_2 & \underline{0} & R_1\underline{h}_3 \\ R_2\underline{h}_1 & R_2\underline{h}_3 & \underline{0} \\ \underline{0} & R_3\underline{h}_2 & R_3\underline{h}_1 \end{bmatrix} \begin{bmatrix} H_{12} & & \bigcirc \\ & H_{23} & \\ \bigcirc & & H_{31} \end{bmatrix}^{-1} \dot{\underline{\phi}} = D H^{-1} \dot{\underline{\phi}} \tag{24}$$

where the second line results from substituting Eqs. (16)-(18) and similar terms for $\partial\underline{\phi}_i/\partial\phi_{jk}$. Comparison of Eqs. (8) and (24) reveals that

$$\dot{\underline{\phi}} = H\underline{\lambda} = H\underline{\lambda}(\underline{\phi}) \tag{25}$$

which is a nonlinear first-order differential equation in $\underline{\phi} = (\phi_{12}, \phi_{23}, \phi_{31})^T$, since $\underline{\lambda}$ is an implicit function of $\underline{\phi}$ by virtue of Eq. (19). Since H is constant for a fixed angular momentum requirement, the equilibrium condition, $\underline{\lambda} = \underline{0}$ falls out immediately.

To investigate stability about an equilibrium point $\underline{\phi}_E$ we first linearize Eq. (25) and obtain

(26) $$\dot{\underline{\Phi}} = A\underline{\Phi}$$

where

(27) $$\underline{\Phi} \equiv \underline{\phi} - \underline{\phi}_E$$

and

(28) $$A = H \left[\frac{\partial \underline{\lambda}^T}{\partial \phi} \right]^T_{\underline{\phi}=\underline{\phi}_E}$$

is a matrix of first partial derivatives of $\underline{\lambda}$ with respect to $\underline{\phi}$. The system defined by Eqs. (26)-(28) is assumed to represent the rotation law dynamics in a region S about an equilibrium $\underline{\Phi}=\underline{0}$. If there exists a positive definite function $V(\underline{\Phi})$ whose derivative in a neighborhood R about $\underline{\Phi}=\underline{0}$ ($R \epsilon S$) is negative-definite, then $\underline{\Phi}=\underline{0}$ is asymptotically stable.[3] Moreover, if the derivative of $V(\underline{\Phi})$ is positive-definite in R then $\underline{\Phi}=\underline{0}$ is completely unstable.

Now consider the positive-definite function

(29) $$V(\underline{\Phi}) = \frac{1}{2} \underline{\Phi}^T \underline{\Phi}$$

where

(30) $$\dot{V}(\underline{\Phi}) = \underline{\Phi}^T \dot{\underline{\Phi}} = \underline{\Phi}^T A \underline{\Phi}$$

From Eq. (19) we have that

(31) $$-K_R H \frac{\partial P}{\partial \underline{\phi}} = \underline{\lambda}$$

The derivative of Eq. (31) with respect to $\underline{\phi}$ and evaluation at $\underline{\phi}=\underline{\phi}_E$ yields

$$-K_R H P_{\phi\phi} = \left[\frac{\partial}{\partial \underline{\phi}} \underline{\lambda}^T\right]_{\underline{\phi}=\underline{\phi}_E} \tag{32}$$

where

$$P_{\phi\phi} \equiv \left[\frac{\partial}{\partial \underline{\phi}} \left(\frac{\partial P}{\partial \underline{\phi}}\right)^T\right]_{\underline{\phi}=\underline{\phi}_E} \tag{33}$$

is the symmetric 3 x 3 matrix of second derivatives of P with respect to $\underline{\phi}$. Use of Eqs. (28) and (32) in Eq. (30) yields

$$\dot{V}(\Phi) = -K_R \underline{\Phi}^T B \underline{\Phi} \tag{34}$$

where

$$B \equiv H P_{\phi\phi} H = -(1/K_R)\, A \tag{35}$$

Thus $\dot{V}$ is negative-definite if B is a positive definite matrix. Since H is diagonal with positive elements the definiteness of B is determined by $P_{\phi\phi}$. At $\underline{\Phi}=\underline{0}$, $P_{\phi\phi}$ is positive-definite ($P_{\phi\phi}>0$) if P is a minimum and negative-definite ($P_{\phi\phi}<0$) if P is a maximum. Hence $\underline{\Phi}=\underline{0}$ is asymptotically stable in R if $P_{\phi\phi}>0$, but unstable in R if $P_{\phi\phi}<0$.

Although these results are based on a linear model of Eq. (25) the global stability question can be easily investigated for 2 CMGs including the case of multiple equilibria. For 2 CMGs λ and ϕ are scalars so that typical dynamical behavior can be represented graphically as in Fig. (2) which illustrates four equilibria. Clearly ϕ_{E1} and ϕ_{E3} are unstable while ϕ_{E2} and ϕ_{E4} are asymptotically stable over the ranges $\phi_{E1}<\phi<\phi_{E3}$ and $\phi_{E3}<\phi<\phi_{E1}+360°$ respectively. Simulation results have confirmed these properties and indicate that they probably prevail for 3 CMGs although we were not able to evaluate boundaries separating domains of attraction between multiple equilibria. For 2 CMGs the domain of attraction for an asymptotically stable equilibrium extends over the entire rotation interval between its two adjacent unstable equilibria.*

---

*If only two equilibria exist, the domain of attraction for the asymptotically stable one is the entire rotation interval (excluding the point of unstable equilibrium).

3.0 Allowable Gimbal Angle Space

We now address the question of portraying the allowable range of gimbal angles consistent with momentum magnitude (H) and direction ($\underline{h}$) requirements which the CMGs must satisfy. Three degrees-of-freedom (DOF) remain to be specified with 3 CMGs operational and one DOF with 2 CMGs. This can all be illustrated in terms of gimbal angle maps for constant $\underline{h}$ with H and the independent variables corresponding to the available DOF as parameters. These will also be useful for subsequent discussion of equilibrium properties.

In the development for 3 CMGs we will not use the rotation angles ($\phi_{12}, \phi_{23}, \phi_{13}$) about the gyro pairs as independent variables. Instead we define an alternate set of variables based on Fig. 3, which illustrates the possible orientation of three unit momentum vectors ($\underline{h}_i, \underline{h}_j, \underline{h}_k$) about their vector sum.*

$$\underline{h}_t \equiv H\underline{h} = \underline{h}_i + \underline{h}_j + \underline{h}_k = \underline{h}_i + \underline{h}_{jk} \qquad 0 \leq H \leq 3 \tag{36}$$

The orientation of $\underline{h}_i$ (selected arbitrarily) can be specified in terms of

α = angle between $\underline{h}_i$ and $\underline{h}$

ϕ = rotation of $\underline{h}_i$ (and $\underline{h}_{jk}$) about $\underline{h}$

The orientation of $\underline{h}_j$ and $\underline{h}_k$ depends on angles (γ, β, ψ) where

γ = angle between $\underline{h}_{jk}$ and $\underline{h}$

β = angle between $\underline{h}_{jk}$ and both $\underline{h}_j$ and $\underline{h}_k$

ψ = rotation of $\underline{h}_j$ and $\underline{h}_k$ about $\underline{h}_{jk}$

---

*Here (i,j,k) are not associated with any particular gyro so the results may be kept general. Later we use i=1, j=2, k=3 to represent Skylab CMGs 1,2, and 3.

The angles β and γ will be shown to be a function of H and α. Hence three independent variables (α,ϕ,ψ) along with H and $\underline{h}$ suffice to define the orientation of $\underline{h}_i$, $\underline{h}_j$, $\underline{h}_k$ uniquely. For 2 CMGs the independent variables reduce to one, namely ϕ. The geometrical reference for $\psi=0$ and $\phi=0$ will be defined later.

3.1 Evaluation of Constraints Due to H (3 CMGs)

In general ϕ and ψ are independent of H but α is not. If we define H_{jk} as the magnitude of $\underline{h}_j+\underline{h}_k$, then from Fig. 3 we can write

$$H_{jk}^2 = H^2 + 1 - 2Hc\alpha \qquad 0\leq H_{jk}\leq 2 \tag{37}$$

or

$$c\alpha = \frac{H^2 + 1 - H_{jk}^2}{2H} \tag{38}$$

A plot of α vs H_{jk} with H as a parameter is shown in Fig. 4. If $H\leq 1$, α can be anywhere in the range $0°\leq\alpha\leq 180°$, regardless of H_{jk}. For $H>1$ the maximum value of α corresponds to $H_{jk}=2$. Consequently

$$\text{(3 CMGs)} \qquad \alpha_{max} = \begin{cases} 180° & H\leq 1 \\ \cos^{-1}\left(\frac{H^2-3}{2H}\right) & H>1 \end{cases} \tag{39}$$

This represents the maximum cone angle about $\underline{h}$ which a gyro momentum vector may have for a given H.

Referring to Fig. 3 again we note that

$$H_{jk} = s\alpha/s\gamma = 2c\beta \tag{40}$$

Thus,

$$\beta = \cos^{-1}(H_{jk}/2) \qquad 0 \leq \beta \leq 90° \tag{41}$$

and

$$\gamma = \sin^{-1}(s\alpha/H_{jk}) \qquad \begin{cases} 0 \leq \gamma \leq 180° & H \leq 1 \\ 0 \leq \gamma \leq 90° & H > 1 \end{cases} \tag{42}$$

Curves of β and γ vs H_{jk} are shown in Fig. 4. Note that $\gamma=\beta$ for H=1. Evaluation of β and γ follows from specifying α and H which determine H_{jk} from Eq. (37).

While α specifies the angle between $\underline{h}_i$ and $\underline{h}$, it is also of interest to consider the angles between $(\underline{h}_j, \underline{h}_k)$ and $\underline{h}$. It is easy to show that if*

$$\alpha_i = \alpha \tag{43}$$

then

$$c\alpha_j = c\beta c\gamma + s\beta s\gamma c\psi \tag{44}$$

and

$$c\alpha_k = c\beta c\gamma - s\beta s\gamma c\psi \tag{45}$$

Curves of (α_j, α_k) vs α are shown in Fig. 6 for various H and ψ. Note that $\alpha_j = \alpha_k$ if ψ=90° or 270° and the isogonal distribution ($\alpha_i=\alpha_j=\alpha_k=\alpha$) also obtains, if $\alpha=\cos^{-1}(H/3)$. This point (I) is labeled in Fig. 5. Note that only one independent variable (ϕ) remains in the isogonal orientation, since α and ψ have been specified.

3.2 Evaluation of Constraints Due to H (2 CMGs)

For the two CMG pairs $(\underline{h}_i, \underline{h}_j)$ or $(\underline{h}_i, \underline{h}_k)$ we may dispense with ψ and set $\gamma=\alpha$ and $\beta=0$. For the pair $(\underline{h}_j, \underline{h}_k)$ we may dispense with ψ and set $\gamma=\alpha_i=0$ and regard β as α. See Fig. 3. In all cases α is constrained by

---

*See Fig. (B-1) associated with Appendix (B-1).

(46) $$c\alpha = H/2 \qquad 0 \leq H \leq 2$$

so that

(47) (2 CMGs)

$$\alpha_{max} = 90° \qquad (H=0)$$

The rotation ϕ is the only independent variable.

3.3 Gimbal Angle Maps

Geometrically the unit momentum vector $\underline{h}_\ell$ for each gyro (ℓ=1,2,3) can be located on a cone with axis $\underline{h}$ and cone half-angle α_ℓ as illustrated in Fig. 6a. The cone base represents the locus of points defined by the tip of $\underline{h}_\ell$ for a given α_ℓ. It is desired to map this locus in gimbal angle space for each gyro. This will provide curves of δ_I vs. δ_O for a given $\underline{h}$ and various α_ℓ where δ_I and δ_O (I=1,3,5; O=2,4,6) are the symmetric* inner and outer gimbal angles defined in Eq. (1).

Consider a sphere with an equator defined by the plane normal to the outer gimbal axis. Now δ_I and δ_O represent latitude and longitude on this sphere. Consider a second sphere with its equator defined normal to $\underline{h}$. From the above discussion the desired

---

*i.e. relative to gimbal stops.

locus (cone base) corresponds to constant latitude circles on the second sphere. See Fig. 6b. Now let the spheres be superimposed with the polar axes displaced by an angle ρ_ℓ (which can be specified given $\underline{h}$ and ℓ = 1,2 or 3). The desired locus is then a curve of constant latitude on the second sphere mapped on to the first in terms of latitude and longitude (δ_I, δ_O). A planar plot of δ_I vs. δ_O for various α_ℓ is entirely analogous to a rectilinear plot of latitude circles from the earth's celestial sphere in terms of ordinary geographical latitude and longitude.*

A gimbal angle map for each gyro is shown in Fig. 7 where $\underline{h}=(0,-.866,.5)^T$,** and α_ℓ is incremented in 15° steps over $0° \leq \alpha \leq 180°$. A portion of gimbal angle space is not available due to mechanical gimbal stops as indicated by shading in Fig. 7.*** The points corresponding to α_ℓ = 0° and α_ℓ = 180° are termed the pole (P) and anti-pole (AP). They designate the gimbal angles for $\underline{h}$ parallel or anti-parallel to $\underline{h}$. Of course P becomes AP and vice-versa if $\underline{h}$ reverses. The pole gimbal angles $\underline{\delta}_p$ can be evaluated from Eq. (B-2) in Appendix B. Setting $\underline{h}_\ell = \underline{h}$ (ℓ=1,2,3) yields

$$(48) \qquad \underline{\delta}_p = \begin{Bmatrix} \delta_{p1} \\ \delta_{p2} \\ \delta_{p3} \\ \delta_{p4} \\ \delta_{p5} \\ \delta_{p6} \end{Bmatrix} = \begin{Bmatrix} -\sin^{-1}(h_z) \\ \tan^{-1}(-h_y/h_x) - 45° \\ -\sin^{-1}(h_x) \\ \tan^{-1}(-h_z/h_y) - 45° \\ -\sin^{-1}(h_y) \\ \tan^{-1}(-h_x/h_z) - 45° \end{Bmatrix}$$

---

*In that case ρ_ℓ = 23.5°, the angle between the earth's geographical and celestial polar axes.

**Numerical values of $\underline{h}$ will always be given in vehicle coordinates (x_v, y_v, z_v).

***The distortion inherent in a rectilinear plot of latitude and longitude causes the excluded region within inner gimbal stops to appear disproportionately large compared to that within outer gimbal stops. For Skylab, gimbal stops are at $\delta_I = \pm 80°$ and $\delta_O = \pm 175°$.

where h_x, h_y and h_z are the components of $\underline{h}$ along vehicle (geometric) axes (x_v, y_v, z_v). The various loci on the gimbal angle maps can also be described analytically. It is easy to show that

$$\delta_O = \delta_{pO} \pm \cos^{-1}\left(\frac{c\alpha_\ell + c\rho_\ell s\delta_I}{s\rho_\ell c\delta_I}\right) \tag{49}$$

$$90° - (\rho_\ell - \alpha_\ell) \leq \delta_I \leq 90° - (\rho_\ell + \alpha_\ell)$$

where ρ_ℓ is the angle between $\underline{h}$ and a gyro outer gimbal axis. For the Skylab CMG configuration shown in Fig. 1 each outer gimbal axis is parallel to one of the geometric axes so that

$$c\rho_\ell = \begin{cases} h_z & \ell = 1 \\ h_x & \ell = 2 \\ h_y & \ell = 3 \end{cases} \tag{50}$$

The $\pm$ signs in Eq. (49) correspond to the segments of the locus on either side of $\delta_O = \delta_{pO}$.

3.4 Allowable Gimbal Angles Ranges

Gimbal angle maps as in Fig. 7 illustrate typical loci for each gyro which depend only on $\underline{h}$ since this establishes the poles $\underline{\delta}_p$. The allowable regions in gimbal space are imposed by H, since this determines α_{max} for any gyro according to Eqs. (39) and (47). For 2 CMGs the allowable range is along a single α_ℓ locus determined by H with ϕ the only free parameter. For 3 CMGs the entire region bounded by the $\alpha_\ell = \alpha_{max}$ locus is available to one gyro. The region available to the other two is generally within a band determined by α, ψ and H. See Fig. 5. However, if α and ψ are fixed, all α_ℓ are fixed and only ϕ remains free. In other words the distribution of the $\underline{h}_\ell$ (ℓ=1,2,3) relative to $\underline{h}$ and each other is fixed, but the composite orientation about $\underline{h}$ is not.

Bifurcation of the allowable gimbal angle range may occur depending on the pole locations and H. This can be noted in Fig. 7 for CMG 2 when $0°<\alpha_2<90°$ and again in Fig. (13) for CMG 2 where H = 2 and $\alpha<75.5°$. This effect leads to multiple equilibria for the rotation law, although it is not a necessary condition as will be observed later. The extent of bifurcation for a particular gyro usually diminishes or even disappears as H becomes small or $\underline{h}$ approaches its inner gimbal axis ($\delta_{pI}\rightarrow 90°$, I=1,3,5).

With Skylab in the solar-inertial mode* the predominant orientation of $\underline{h}$ is normal to the orbital plane due to the cyclic component of gravity-gradient torque. In that case

$$\underline{h}^v \approx \pm \begin{Bmatrix} c\eta_x s\nu_z \\ c\eta_x c\nu_z \\ -s\eta_x \end{Bmatrix} \tag{51}$$

The corresponding poles $\underline{\delta}_p$ are denoted by ⊕ and ⊖ in Fig. 8 for $-75°\leq\eta_x\leq 75°$. The loci between ⊕ and ⊖ represent the instantaneous pole migrations from ⊕ to ⊖, if the gravity-gradient bias momentum component dominates, when the cyclic component passes through zero. If the bias component is small the transition time is rather short (e.g. 30 sec for $H_{bias}<0.1$).

With Skylab in the ZLV/XIOP mode** the orientation of $\underline{h}$ is essentially normal to the orbital plane and $\underline{h}\approx(0,1,0)^T$. The corresponding poles are designated in Fig. 9 along with regions denoting the dominant pole locations during ZLV/XIOP entry and exit maneuvers.

---

*In the SI mode z_v points to the sun and x_v is rotated about by an angle ν_z from the orbital plane.[1] Here ν_z is based on placing the x principal axis in the orbital plane for all η_x. See PDD Eq. 15.3.3[1]. The sunline inclination to the orbital plane is η_x where $\eta_x>0$ with the sunline below the orbital plane at noon.

**In the ZLV/XIOP mode z_v points toward the earth's center and x_v is in the orbital plane.

4.0 Equilibrium Evaluation and Potential Problem Areas

It has been shown that equilibrium occurs for the Skylab CMG rotation law whenever $\underline{\lambda}$, as defined by Eq. (9), is zero. This condition corresponds to extrema of a quadratic function of gimbal angles, $P(\underline{\delta})$ in Eq. (23). It has also been established that the equilibria $\underline{\delta}_E$ are asymptotically stable in some neighborhood about $\underline{\delta}_E$ if $P(\underline{\delta}_E)$ is a minimum and unstable if $P(\underline{\delta}_E)$ is a maximum.

One of our objectives was to systematically determine the number and location of stable equilibria given the angular momentum parameters, H and $\underline{h}$.* While time has precluded an encyclopedic treatment, illustrative results of that effort are given below. This is followed by an assessment of some potential difficulties which may arise in the current rotation law implementation.

4.1 Equilibrium Loci in Gimbal Angles Space

Two methods were utilized in locating equilibria, one based on a Skylab CMG simulation[4] and the other on systematic scanning of the (α,ϕ,ψ) parameters to test $\underline{\lambda} = \underline{0}$ in allowable gimbal angle space. Both simulation and scanning were used with 3 CMGs since they proved to be complimentary whereas only parameter scanning (by ϕ) was needed for 2 CMGs.

4.1.1 Three CMGs

With the simulation approach a slowly varying ramp torque of fixed direction was applied to the vehicle to vary H over $0 \leq H \leq 3$. Since the torque variation was slow compared to the rotation law dynamics, the CMGs tracked the equilibria as a function of H. A plot of the gimbal angles corresponding to equilibria for various H (with $\underline{h}$ fixed) is defined as an equilibrum locus. Figs. (10) and (11) show $\underline{\delta}_E$ loci for 3 CMGs with $\underline{h}$ at various orientations in the (y_v,z_v) and (x_v,y_v) planes.** These are defined by θ where $\theta = (0°,90°,180°,270°)$ denotes $\underline{h}$ directed along $(+y_v,-z_v,-y_v,+z_v)$ for Fig. (10) and along $(+y_v,-x_v,-y_v,+x_v)$ for Fig. (11). Intermediate values of θ are also shown.

---

*Use of the term, stable equilibrium, hereafter is only for brevity. Strictly speaking, we mean asymptotically stable equilibrium.

**Similar families of $\underline{\delta}_E$ loci can be generated for $\underline{h}$ in planes intermediate to the (y_v,z_v) and (y_v,x_v) planes. The patterns are somewhat of a composite between Figs. (10) and (11).

All loci contain the origin (where H=0), since $\underline{\delta}_E = \underline{0}$ follows from Eq. (9). The outer end point on each locus (where H=3) corresponds to the pole ($\underline{\delta}_p$) for that $\underline{h}$. Note that the $\underline{\delta}_p$ follow the pattern of the dominant poles ⊕, ⊖ observed earlier in Fig. (8), which arise in the solar inertial mode.

A simulation approach provides a convenient means for identifying the $\underline{\delta}_E$ loci emanating from the origin for arbitrary momentum conditions. However, it does not begin to exhaust the possible range of allowable gimbal angles satisfying $\underline{h}_t = H\underline{h}$. For this the parameter scanning method was useful and was instrumental in determining additional equilibria. Once one of the multiple equilibria was identified the simulation was initialized to this condition and H varied (with $\underline{h}$ fixed) to determine the extent of this $\underline{\delta}_E$ locus in gimbal space. Some additional loci for $\underline{h}$ in the (y_v, z_v) plane are shown in Fig. (12) together with the corresponding loci emanating from the origin previously shown in Fig. (10).

The $\underline{\delta}_E$ loci in Fig. (12) are a result of bifurcation of the allowable gimbal space due to the location of $\underline{\delta}_p$ for CMG 2. The bifurcation is illustrated by the gimbal angle map in Fig. (13) for H = 2 and $\underline{h} = (0,-.866,.5)^T$. Points A and A' in Figs. (12) and (13) denote corresponding $\underline{\delta}_E$. Similar bifurcation and resulting multiple $\underline{\delta}_E$ also result when $\underline{h}$ is located near the anti-nominal orientation of either CMG 1 or 3.*

Multiple $\underline{\delta}_E$ are not only the result of the bifurcation effect, although this seems to be the dominant cause for 3 CMGs. An example of multiple $\underline{\delta}_E$ not due to bifurcation is shown in Fig. (14). For H = 0 the origin $\underline{\delta} = \underline{0}$ appears to be a unique stable equilibrium.** Although we could not demonstrate this analytically, scanning of gimbal space with (α,ϕ,ψ) did not prove otherwise.

---

*The anti-nominal orientation, $\underline{\delta} = (0,\pi,0,\pi,0,\pi)^T$, is opposite to the nominal position, $\underline{\delta} = \underline{0}$.

**Although the anti-nominal orientation is an equilibrium for H = 0, it is unstable.

Multiple equilibria occurring within interior gimbal space are probably of little concern. However, the existence of $\underline{\delta}_E$ loci which extend to a gimbal stop is of importance since a gyro operating on this segment will encounter the stop for sufficiently large H. For a purely cyclic momentum variation 3 CMGs tend to operate about the origin with the excursion away from it dependent on $\underline{\delta}_p$ and H_{max} per cycle. With both cyclic (H_c) and bias (H_b) components present, particularly when orthogonally oriented, rapid changes in $\underline{\delta}_E$ can occur as $H_c \to 0$, if H_b is sufficiently large. Compare Figs. (10) and (11). This phenomenon or other momentum transients, as in maneuvers, can provide the mechanism for acquiring an equilibrium on an undesirable $\underline{\delta}_E$ locus.

4.1.2 Two CMGs

To determine stable equilibria for 2 CMGs it is only necessary to scan over ϕ for given momentum conditions $(H,\underline{h})$ and test for $P(\underline{\delta})$ = minimum or conversely, $\partial\lambda_i/\partial\phi < 0$ at $\lambda_i = \overline{0}$ $(i=1,2,3)$. The applicable λ_i are obtained from Eqs. (9) and (10) as

$$\lambda_1 = (R_1\underline{h}_2)^T\underline{\delta}_1 + (R_2\underline{h}_1)^T\underline{\delta}_2 \qquad \text{CMGs 1 \& 2}$$

$$\lambda_2 = (R_2h_3)^T\underline{\delta}_2 + (R_3\underline{h}_2)^T\underline{\delta}_3 \qquad \text{CMGs 2 \& 3} \tag{52}$$

$$\lambda_3 = (R_3\underline{h}_1)^T\underline{\delta}_3 + (R_1\underline{h}_3)^T\underline{\delta}_1 \qquad \text{CMGs 3 \& 1}$$

where $\underline{\delta}_1=(\delta_1,\delta_2)^T$, $\underline{\delta}_2=(\delta_3,\delta_4)^T$ and $\underline{\delta}_3=(\delta_5,\delta_6)^T$. Figs. (15)-(17) show the gimbal angle maps and $\underline{\delta}_E$ loci corresponding to each gyro pair for $\underline{h} = \pm(0\ -.866,.5)^T$. The poles corresponding to $\pm$ are denoted by $\oplus$ and $\ominus$.* For 2 CMGs all equilibria, stable and unstable, are easily represented on the same plot. Stable $\underline{\delta}_E$ loci are denoted by the solid heavy lines and unstable loci by dashed lines. The latter, which correspond to $P(\underline{\delta})$ = maximum (or $\partial\lambda_i/\partial\phi>0$ at $\lambda_i = 0$), effectively demarcate the zones of attraction of stable equilibria on a particular α contour.

---

*The maps are similar to Fig. (7) except that here α contours (H=constant) extend only over $0° \le \alpha \le 90°$ for 2 CMGs. The notations + and - on numerical values of α in Figs. (15)-(17) designate the contours applicable to $\oplus$ and $\ominus$.

Multiple equilibria are common for 2 CMGs and as many as 4-5 different segments have been observed on similar plots. In all cases there is a major locus which connects the poles, although it never includes the origin unless $\underline{h}$ has the anti-nominal orientation of the missing gyro. The additional loci may or may not extend to a gimbal stop. Corresponding loci for the gyro pairs are labeled I, II, III, etc. in Figs. (15)-(17). Examples of equilibria for other $\underline{h}$ are shown in Fig. (18) for CMGs 1 and 2. Certain symmetries arise so that patterns of loci for one gyro pair will occur for another with a different $\underline{h}$. For example, δ_E loci for CMGs 2 and 3 with $h=(0,-.5,.866)^T$ are inverted images of those for CMGs 2 and 1 respectively, in Fig. (15).

It should be recalled that in the current Skylab rotation law implementation the elements of the $R_i\underline{h}_j$ $(i\neq j)$ in Eq. (52) are limited in magnitude to a constant, SL (currently SL=.04).* The $\underline{\delta}_E$ loci for CMGs 1 and 2 with limiting for $\underline{h} = \pm(0,-.866,.5)^T$ are shown in Fig. (19) for comparison with Fig. (15). Here 10 loci appear compared to 5 without SL limiting. It might also be noted that varying H so as to move to one pole and then back to the other will always result in a gimbal stop encounter, regardless of initial gimbal angles. This is partly a consequence of no single (i.e. major) locus connecting the two poles.

4.2 Potential Problem Areas

Multiple stable equilibria have been shown to exist for both 2 and 3 CMGs. The nature of the phenomena is such that some $\underline{\delta}_E$ loci extend out to gimbal stops. Operation on one of these segments can result in a gimbal stop encounter which leads to TACS** activation if H increases and spacecraft attitude error grows sufficiently. With 3 CMGs the situation is less uncertain since ultimate recovery to the origin obtains whenever $H\to 0$.*** With 2 CMGs $\underline{\delta}_E = 0$ generally does not exist and multiple equilibria often occur about H=0 ($\alpha=90°$). Furthermore it is possible to acquire an equilibrium on an undesirable $\underline{\delta}_E$ locus by a normal Skylab CMG operation, i.e. caging.

---

*This does not change the condition for equilibrium ($\underline{\lambda}=\underline{0}$) or stability properties, although $P(\delta)$ is no longer a quadratic function of gimbal angles.

**TACS = Thruster Attitude Control System

***This is based on our assertion (from computational evidence) that $\underline{\delta}_E = \underline{0}$ appears to be a unique equilibrium and from stability results, therefore globally asymptotically stable.

When caging is commanded, the gyros are first reset to the nominal orientation ($\underline{\delta}=\underline{0}$) and then TACS is activated such that the gyros achieve a desired momentum state $\underline{h}_t = H\underline{h}$. Hence, caging with 3 CMGs results in acquiring the major $\underline{\delta}_E$ locus, a priori, but not necessarily for 2 CMGs. As an example, the equilibria acquired by CMGs 1 and 2 in caging to $\underline{h} = (0,-.866,.5)^T$ for $0.2 \leq H \leq 1.8$ with and without SL limiting are plotted in Fig. (20). It is evident that the undesirable loci (II) in Figs. (15) and (19) are acquired for a considerable range of H in each case ($0.2 \leq H \leq 1.2$). This $\underline{h}$ also arises in the solar-inertial mode for $\eta_x = +30°$. Thus, if CMGs 1 and 2 were caged to this condition shortly after orbital 6 AM ($H<1.2$), CMG 2 would encounter its outer gimbal stop near orbital noon with just the nominal external disturbance environment active.* Similar results occur for CMGs 1 and 2 over a range of η_x, at least over $30° \leq \eta_x < 45°$ and for CMGs 2 and 3 over $45° < \eta_x \leq 60°$. Other examples of gimbal stop encounters for 2 CMGs could also be cited; some are to be published.[5]

It should be noted that if in caging, the CMGs had acquired the major locus (I) connecting the poles in Fig. (15) for all H, then no stop encounter, as outlined above, could occur. This is the motivation for a simple modification of the rotation law, considered next, which would lead to acquisition of the major locus in caging operations or in transferring to any desired momentum state.

5.0 Possible Rotation Law Modification

It was observed in Section 4 that all major equilibrium-loci for 3 CMGs include the origin. This provides a natural focal point, as H decreases, which is consistent with the rotation law's fundamental purpose: to avoid gimbal stop encounters. Such is not the case for 2 CMGs where $\underline{\delta}_E = \underline{0}$ does not exist for arbitrary $\underline{h}$. A question arises as to whether a dynamic origin ($\underline{\delta}_N$) based on

---

*The momentum requirement is such that the gimbal angles must proceed toward the ⊖ pole and the route followed is along $\underline{\delta}_E$ loci II→IV→V in Figs. (15) and (19). With venting torque or momentum biasing present the likelihood for a stop encounter could be enhanced or possibly avoided depending on conditions.

desired momentum conditions (H,$\underline{h}$) could be utilized to increase the likelihood of operation on a major locus which is essentially always interior* to the useful gimbal angle space. Initial results have proved encouraging in that it is possible with only slight modification of the current rotation law implementation to acquire the major locus for all H during caging operations with 2 CMGs.

Our approach was to omit SL limiting and simply modify $\underline{\lambda}$ in Eqs. (9) and (31) such that

$$(53) \qquad -K_R \, H\frac{\partial P}{\partial \underline{\phi}} = \underline{\lambda} \equiv -K_R \, D^T Q(\underline{\delta} - \underline{\delta}_N)$$

where $\underline{\delta}_N$ is some set of gimbal angles to be defined. By arguments parallel to Section 2.2 it follows that

$$(54) \qquad \frac{\partial P}{\partial \underline{\phi}} = \frac{\partial}{\partial \underline{\phi}} \left[\frac{1}{2}(\underline{\delta}-\underline{\delta}_N)^T Q(\underline{\delta}-\underline{\delta}_N) \right]$$

so that

$$(55) \qquad P(\underline{\delta}) = \frac{1}{2} \, (\underline{\delta}-\underline{\delta}_N)^T Q(\underline{\delta}-\underline{\delta}_N)$$

is a quadratic function of gimbal angles relative to an origin at $\underline{\delta} = \underline{\delta}_N$. Hence, for 2 CMGs the equilibrium condition $\lambda_i=0$ and all stability results ($\partial\lambda_i/\partial\phi<0$ for δ_E asymptotically stable and $\partial\lambda_i/\partial\phi>0$ for δ_E unstable) are unaffected.**

---

*The exception is for a small segment of a major locus near a pole which lies within a gimbal stop region. However, this is of minor significance since the gyros would be nearly saturated (H→2) in this orientation.

**If SL limiting were present $P(\underline{\delta})$ would not necessarily be a quadratic function of gimbal angles, although $P(\delta)$, whatever it is, would still have an extremum at $\lambda=0$ by virtue of Eq. (53).

The manner of choosing $\underline{\delta}_N$ is, of course, a designers' option. One approach would be to set $\underline{\delta}_N$ equal to the set of gimbal angles on the major locus corresponding to $\underline{\delta}_N = \underline{0}$ for a particular $\underline{h}$ and H. Given a large memory computer to store possible $\underline{\delta}_N$ for the 3 pairs of CMGs and all $(\underline{h},H)$, this would be theoretically possible. As a practical matter it would be more useful if something close but computationally feasible were utilized.

For the purposes here we have chosen $\underline{\delta}_N$ from simple geometric arguments which are discussed in more detail in Appendix C. Basically the components of $\underline{\delta}_N$ are those gimbal angles which each gyro would have with its momentum vector in a plane normal to the plane formed by $\underline{h}$ and its outer gimbal axis. (See Fig. C-1.) This is defined by

$$(56) \qquad \underline{\delta}_{N\ell} = \begin{Bmatrix} \delta_{N(2\ell-1)} \\ \delta_{N(2\ell)} \end{Bmatrix} = \begin{Bmatrix} -\sin^{-1}(c\rho_\ell c\alpha) \\ \delta_{P(2\ell)} - \nu\tan^{-1}\left(\frac{\tan\alpha}{s\rho_\ell}\right) \end{Bmatrix} \quad \ell=1,2,3$$

where

$$(57) \qquad \nu = \begin{cases} +1 & \delta_{p(2\ell)} > 0 \\ -1 & \delta_{p(2\ell)} < 0 \end{cases}$$

The parameter α is obtained from H by Eq. (46) and the quantities $\delta_{p(2\ell)}$ and ρ_ℓ are specified by $\underline{h}$ in Eqs. (48) and (50).

The resulting equilibrium loci for CMGs 1 and 2 are shown in Fig. (21) for $\underline{h} = \pm(0,-.866,.5)^T$. The major locus is seen to be a satisfactory approximation to that in Fig. (15). Gimbal angles acquired in caging to $\underline{h} = (0,-.866,.5)^T$ for $0.2 \leq H \leq 1.8$ are shown in Fig. (22) along with the major locus for

$\underline{\delta}_N = \underline{0}$ and $\underline{\delta}_N \neq \underline{0}$. If $\underline{\delta}_N$ is set to zero in the rotation law after caging, the CMGs shift slightly to the $\underline{\delta}_N = \underline{0}$ major locus. This demonstrates the feasibility of acquiring the desired equilibrium location in gimbal angle space with relatively modest impact on the current rotation law formulation. The limiting operation (by SL), presumably introduced for transient behavior considerations, would be better served by gain-limiting of K_R. As might be expected, the dynamic origin approach with SL limiting did not substantially alter the results from those in Fig. (20) where $\underline{\delta}_N = \underline{0}$.

6.0 Suggested Areas for Further Research

It may be useful to future investigators to identify at this point some areas which appear to us to merit attention. We have divided these into areas of perhaps more immediate concern and those of longer range interest.

A. Current Interest

1. Catalog of Equilibrium Loci - $\underline{\delta}_E$ loci are dependent only on the momentum parameters and the particular CMGs involved. Availability of a permanent record or a stored program for CRT display could support simulators or ground monitors in anticipating CMG gimbal angle performance from expected momentum requirements.

2. SL Limiting Effects - The implications for gimbal angle performance with SL limiting need to be more fully examined. Our investigations with both 2 and 3 CMGs indicate an increase in the number of multiple equilibria and for 2 CMGs, the disappearance of a major $\underline{\delta}_E$ locus in some cases. This is at least part of the cost incurred for some control of transient response with SL limiting. If an adaptive "gain" is warranted, it might better be obtained by modifying K_R as a function of $\underline{\lambda}$, e.g.

$$K_R = \begin{cases} K_R & |\underline{\lambda}'| \leq a \\ \dfrac{a}{|\underline{\lambda}'|} K_R & |\underline{\lambda}'| > a \end{cases} \qquad \underline{\lambda}' \equiv D^T Q \underline{\delta} \tag{58}$$

This at least avoids any impact on equilibrium properties.

3. Dynamic Origin Concept - The dynamic origin ($\underline{\delta}_N$) formulation provides more flexibility to the rotation law, particularly for 2 CMGs. Equilibrium implies minimization of a quadratic function of gimbal angles relative to $\underline{\delta}_N$ which can be selected to be compatible with actual or desired momentum conditions. The specification of $\underline{\delta}_N$ and its application needs to be studied. Appendix C offers one approach.

4. Domain of Attraction for 3 CMG Equilibria - The location of "ridge lines" separating domains of attraction for multiple equilibria was not solved for 3 CMGs. One approach which might be pursued follows from the observation that on a contour of constant $P(\delta)$, a point on a ridge line must satisfy the condition.

$$(59) \qquad \left|\frac{\partial P}{\partial \underline{\phi}}\right|^2 = \left(\frac{\partial P}{\partial \phi_{12}}\right)^2 + \left(\frac{\partial P}{\partial \phi_{23}}\right)^2 + \left(\frac{\partial P}{\partial \phi_{31}}\right)^2 = \text{minimum; } P = \text{constant}$$

B. Future Interest

1. CMG Mounting Arrangement - Our results are confined to the case of CMGs with orthogonally oriented outer gimbal axes. Other, perhaps better, equilibrium characteristics might be obtained for 2 and 3 CMG operation with different mounting arrangements in each case. If so, a movable frame for optimizing the mounting arrangement among the operational CMGs could be an important consideration for future systems.

2. Gimbal Angle Control Law - In connection with the dynamic origin concept it may be possible to develop a gimbal angle control law which simultaneously accomplishes both CMG steering and gimbal angle management. Knowledge of $\underline{h}_t = H\underline{h}$ required to specify desired gimbal angles at time increment (n+1) from data at (n) is obtained from

$$(60) \qquad (\underline{h}_t)_{n+1} = (\underline{h}_t)_n + (\underline{t}_c - \tilde{\underline{\omega}}\, \underline{h}_t)_n \, \Delta\tau$$

which for sufficiently small $\Delta\tau$ is a valid integration of

$$(61) \qquad \dot{\underline{h}}_t + \tilde{\underline{\omega}}\, \underline{h}_t = \underline{t}_c$$

Here $\underline{t}_c$ is the desired control torque obtained as in Skylab from a linear combination of attitude and rate error ($\underline{\phi}_e, \dot{\underline{\phi}}_e$)

$$(62) \qquad \underline{t}_c = -(A_0 \underline{\phi}_e + A_1 \dot{\underline{\phi}}_e)$$

7.0 Summary and Conclusions

The Skylab CMG rotation law has been investigated to develop an understanding of its implications for gimbal angle management under various angular momentum conditions. The effort was stimulated by the earlier work of Kranton and Chu[6] on CMG control laws. They observed rapid transients in gimbal angle trajectories during simulation studies which suggested the possibility of multiple equilibria. Our objective was to ascertain the conditions for equilibria, determine stability properties and to examine any potential for gimbal stop encounters. We had also hoped to develop a compendium of possible equilibria over a wide range of momentum conditions for both 2 and 3 CMGs. Time has not permitted us to complete the latter work but we have included a number of illustrative examples and some techniques for evaluation of equilibria which future investigators might wish to utilize.

The rotation law formulation in terms of gimbal angles $\underline{\delta} = (\delta_1 \ldots \delta_6)^T$ is

$$\dot{\underline{\delta}} = D(\underline{\delta})\underline{\lambda} \tag{63}$$

where

$$\underline{\lambda} = -K_R\, D^T(\underline{\delta})Q\, \underline{\delta} \tag{64}$$

For 3 CMGs $D(\underline{\delta})$ is a 6×3 transformation matrix relating gimbal axes to vehicle axes, Q is a constant 6×6 weighting matrix and K_R is a fixed scalar constant.* An equivalent formulation in terms of the rotations about respective CMG pairs, $\underline{\phi} = (\phi_{12}, \phi_{23}, \phi_{31})^T$, is

$$\dot{\underline{\phi}} = H\underline{\lambda} \tag{65}$$

---

*For 2 CMGs, $D(\delta)$ reduces to 4×1, Q to 4×4 and $\underline{\delta}$ to 1×4 with elements consistent with appropriate pairs of CMGs. Also, $\underline{\lambda}$ becomes a scalar.

where H is a constant (3×3) matrix for fixed momentum magnitude (H) and direction ($\underline{h}$). The correspondence between $\underline{\delta}$ and $\underline{\phi}$ for a fixed rotation sequence among $(\phi_{12}, \phi_{23}, \phi_{31})$, is unique.

The results of this study have established the following theoretical properties:

A. The necessary and sufficient condition for equilibrium ($\dot{\underline{\delta}}=\underline{0}$) is: $\underline{\lambda}=\underline{0}$.

B. Equilibria ($\underline{\delta}_E$) correspond to extrema of a quadratic function of gimbal angles: $P(\underline{\delta}) = (\frac{1}{2})\underline{\delta}^T Q \underline{\delta}$.

C. An equilibrium point ($\underline{\delta}_E$, or correspondingly $\underline{\phi}_E$) is

   1. asymptotically stable in a region (R) about $\underline{\delta}_E$ if $P(\underline{\delta}_E)$ is a minimum and unstable if $P(\underline{\delta}_E)$ is a maximum, or equivalently,

   2. asymptotically stable in R if the matrix,

$$H \left[\frac{\partial}{\partial \underline{\phi}} \underline{\lambda}^T \right]^T_{\underline{\phi}=\underline{\phi}_E}, \text{ is negative definite and}$$

   unstable if it is positive definite.

D. For 2 CMGs the domain of attraction about a given $\underline{\phi}_E$ is the entire rotation interval between its adjacent unstable equilibria.*

E. For 3 CMGs and H=0, $\underline{\delta}_E=\underline{0}$ is a unique asymptotically stable equilibrium (based on computational evidence).

Two methods were utilized in evaluating equilibria, one based on a CMG computer simulation[4] and the other on systematic scanning of allowable $\underline{\delta}$ space which varies with momentum parameters (H,$\underline{h}$). The first relies on the asymptotic stability property to locate equilibria and the second on testing $\underline{\lambda}$ or $P(\underline{\delta})$ according to properties A or B at each step in the scanning process. A plot of the asymptotically stable $\underline{\delta}_E$ for fixed $\underline{h}$ define

---

*For 2 CMGs, $\underline{\phi}$ is a scalar.

equilibrium-loci that the CMGs tend to follow in $\underline{\delta}$ space as H varies.

Multiple equilibria were shown to exist for both 2 and 3 CMGs with some "undesirable" loci extending to the gimbal stops, thus creating the potential for stop encounters. Gimbal angle transients can result from the transfer between different $\underline{\delta}_E$ loci for fixed $\underline{h}$ or the transfer between widely separated $\underline{\delta}_E$ for rapidly changing $\underline{h}$. For 3 CMGs a $\underline{\delta}_E$ locus always emanates from the origin ($\underline{\delta}_E = \underline{0}$) where H=0 and terminates at the gimbal angles ($\underline{\delta}_p$) where H=3 (CMG saturation).* For 2 CMGs the major $\underline{\delta}_E$ locus (terminating at $\underline{\delta}_p$) cannot include $\underline{\delta}_E = \underline{0}$ at H=0. In fact multiple equilibria, widely separated in $\underline{\delta}$ space, commonly occur near H=0. Hence, the 3 CMG case has a natural recovery capability (to $\underline{\delta}_E$=0), but the 2 CMG case does not. It has been demonstrated that normal Skylab caging operations for some momentum conditions can lead to acquiring an undesirable locus with subsequent operation leading to a stop encounter.

A simple modification of the rotation law was developed which provides more flexibility for gimbal angle management. This is the dynamic origin concept based on defining $\underline{\lambda}$ in Eq. (63) as

$$\underline{\lambda} = -K_R \, D^T Q \, (\underline{\delta} - \underline{\delta}_N) \tag{66}$$

where $\underline{\delta}_N$ is an arbitrary set of gimbal angles. All of the equilibrium properties, A-E, still apply except $P(\underline{\delta})$ in B becomes $P(\underline{\delta}) = \frac{1}{2}(\underline{\delta}-\underline{\delta}_N)^T Q(\underline{\delta}-\underline{\delta}_N)$ and $\underline{\delta}_E=\underline{0}$ in E becomes $\underline{\delta}_E = \underline{\delta}_N$. A method was presented for selecting $\underline{\delta}_N$ which, for 2 CMGs, leads to acquisition of a major locus in caging operations.

In the present rotation law implementation the elements of $D^T(\underline{\delta})$ in Eq. (63) are limited to a constant (SL).** This

---

*CMG spin angular momenta are normalized to 1. For 2 CMGs $0 \leq H \leq 2$.

**Currently, SL = $.04^{(1)}$.

effectively voids properties B, C1 and perhaps E, although the latter was not demonstrated conclusively. SL limiting has other implications for gimbal angle management since it tends to increase the number of multiple equilibria, particularly for 2 CMGs. It has also been demonstrated that with limiting and appropriate momentum conditions, gimbal stop encounters can always occur regardless of the initial $\underline{\delta}$. Another approach that provides limiting for control of transient response, yet avoids the impact on equilibrium properties, was suggested. (See Section 6.)

Acknowledgement

The authors gratefully acknowledge the efforts of R. W. Grutzner whose programming skills contributed extensively to the acquisition of data for this study.

B. D. Elrod

G. M. Anderson

1022-BDE_mef
GMA_ams

Appendix A

Necessary Condition for Equilibrium

We prove here that

(A-1) $$\underline{\lambda} = 0$$

is the necessary condition for equilibrium.

Suppose that

(A-2) $$\underline{\lambda} \neq 0$$

For equilibrium under this condition it is necessary, from Equation 4, that

$$D\underline{\lambda} = 0$$

For Equation (A-1) to have solutions, other than $\underline{\lambda} = 0$, it is necessary that the rank of D must be less than 3. The rank of D is certainly no greater than 3 since D is a 6x3 matrix. If the rank of D is exactly three, the associated minor can be inverted to yield at once, in (A-2), $\underline{\lambda} = 0$.

There are 20, 3 x 3, minors in D. The determinants of these minors must all be zero for the rank of D to be less than three.

The $R\underline{h}$ elements in D are 2 x 1 vectors. Designating the components of these vectors by subscripts 1 and 2, D may be written

$$(A\text{-}3)\quad D = \begin{bmatrix} (R_1h_2)_1 & 0 & (R_1h_3)_1 \\ (R_1h_2)_2 & 0 & (R_1h_3)_2 \\ (R_2h_1)_1 & (R_2h_3)_1 & 0 \\ (R_2h_1)_2 & (R_2h_3)_2 & 0 \\ 0 & (R_3h_2)_1 & (R_3h_1)_1 \\ 0 & (R_3h_2)_2 & (R_3h_1)_2 \end{bmatrix}$$

Number the rows of D from 1 through 6. Set the determinants of the twenty minors obtained from the combinations of six rows taken three at a time equal to zero. Eleven independent equations result. They are listed along with the rows of D used to form the minor.

$$(A\text{-}4)\quad \begin{matrix}123\\124\\125\\126\end{matrix}\qquad \frac{(R_1h_2)_1}{(R_1h_2)_2} = \frac{(R_1h_3)_1}{(R_1h_3)_2}$$

$$(A\text{-}5)\quad \begin{matrix}341\\342\\345\\346\end{matrix}\qquad \frac{(R_2h_1)_1}{(R_2h_1)_2} = \frac{(R_2h_3)_1}{(R_2h_3)_2}$$

$$(A\text{-}6)\quad \begin{matrix}156\\256\\356\\456\end{matrix}\qquad \frac{(R_3h_2)_1}{(R_3h_2)_2} = \frac{(R_3h_1)_1}{(R_3h_1)_2}$$

$$(A\text{-}7)\quad 135\qquad \frac{(R_1h_2)_1}{(R_1h_3)_1}\ \frac{(R_2h_3)_1}{(R_2h_1)_1}\ \frac{(R_3h_1)_1}{(R_3h_2)_1} = -1$$

(A-8) 136 $$\frac{(R_1h_2)_1}{(R_1h_3)_1}\ \frac{(R_2h_3)_1}{(R_2h_1)_1}\ \frac{(R_3h_1)_2}{(R_3h_2)_2} = -1$$

(A-9) 145 $$\frac{(R_1h_2)_1}{(R_1h_3)_1}\ \frac{(R_2h_3)_2}{(R_2h_1)_2}\ \frac{(R_3h_1)_1}{(R_3h_2)_1} = -1$$

(A-10) 146 $$\frac{(R_1h_2)_1}{(R_1h_3)_1}\ \frac{(R_2h_3)_2}{(R_2h_1)_2}\ \frac{(R_3h_1)_2}{(R_3h_1)_2} = -1$$

(A-11) 235 $$\frac{(R_1h_2)_2}{(R_1h_3)_2}\ \frac{(R_2h_3)_1}{(R_2h_1)_1}\ \frac{(R_3h_1)_1}{(R_3h_2)_1} = -1$$

(A-12) 236 $$\frac{(R_1h_2)_2}{(R_1h_3)_2}\ \frac{(R_2h_3)_1}{(R_2h_1)_1}\ \frac{(R_3h_1)_2}{(R_3h_2)_2} = -1$$

(A-13) 245 $$\frac{(R_1h_2)_2}{(R_1h_3)_2}\ \frac{(R_2h_3)_2}{(R_2h_1)_2}\ \frac{(R_3h_1)_1}{(R_3h_2)_1} = -1$$

(A-14) 246 $$\frac{(R_1h_2)_2}{(R_1h_3)_2}\ \frac{(R_2h_3)_2}{(R_2h_1)_2}\ \frac{(R_3h_1)_2}{(R_3h_2)_2} = -1$$

There are conditions under which elements of D, the Rh terms, may be zero. These are dealt with later. For the present it is assumed that the terms in Equations (A-4) through (A-10) are non-zero.

Let

(A-15)
$$x = \frac{(R_1h_2)_1}{(R_1h_3)_1} = \frac{(R_1h_2)_2}{(R_1h_3)_2}$$
$$y = \frac{(R_2h_3)_1}{(R_2h_1)_1} = \frac{(R_2h_3)_2}{(R_2h_1)_2}$$
$$z = \frac{(R_3h_1)_1}{(R_3h_2)_2} = \frac{(R_3h_1)_2}{(R_3h_2)_2}$$

Equations (A-7) through (A-14) are equivalent to a single equation

$$xyz = -1 \tag{A-16}$$

Setting the determinants of the 20, 3 x 3 minors of D to zero has thus resulted in four Equations, (A-4), (A-5), (A-6) and (A-16).

Let

$$\begin{aligned} \underline{u} &= R_1 \underline{h}_3 \\ \underline{v} &= R_2 \underline{h}_1 \\ \underline{w} &= R_3 \underline{h}_2 \end{aligned} \tag{A-17}$$

Then from Equations (A-15)

$$R_1 \underline{h}_2 = x\,\underline{u};\quad R_2 \underline{h}_3 = y\,\underline{v};\quad R_3 \underline{h}_1 = z\,\underline{w} \tag{A-18}$$

and, therefore

$$D = \begin{bmatrix} x\,\underline{u} & 0 & \underline{u} \\ \underline{v} & y\,\underline{v} & 0 \\ 0 & \underline{w} & z\,\underline{w} \end{bmatrix} \tag{A-19}$$

Insert D from (A-19) into (A-2) to obtain, since $\underline{u}$, $\underline{v}$, and $\underline{w}$ are non-zero,

$$\begin{aligned} x\,\lambda_1 + \lambda_3 &= 0 \\ y\,\lambda_2 + \lambda_1 &= 0 \\ z\,\lambda_3 + \lambda_2 &= 0 \end{aligned} \tag{A-20}$$

Equations (A-20) do not of themselves establish that $\underline{\lambda} = 0$ since setting the determinant of this system equal to zero yields

$$xyz = -1$$

or Equation (A-16). Since the determinant is zero, a non-zero $\underline{\lambda}$ is possible.

Let

(A-21) $$\underline{\gamma} = \begin{pmatrix} \underline{\gamma}_1 \\ \underline{\gamma}_2 \\ \underline{\gamma}_3 \end{pmatrix} = Q_1 \underline{\delta}$$

where

$$\underline{\gamma}_1 = Q_1 \begin{pmatrix} \delta_1 \\ \delta_2 \end{pmatrix}; \quad \underline{\gamma}_2 = Q_1 \begin{pmatrix} \delta_3 \\ \delta_4 \end{pmatrix}; \quad \underline{\gamma}_3 = Q_1 \begin{pmatrix} \delta_5 \\ \delta_6 \end{pmatrix}$$

and

$$Q_1 = \begin{bmatrix} 1 & 0 \\ 0 & .457 \end{bmatrix}$$

From Equations (5), (A-19), and (A-21)

$$\underline{\lambda} = -K_r \, D^T \underline{\gamma}$$

(A-22)
$$= -K_r \begin{bmatrix} x\underline{\gamma}_1^T\underline{u} + \underline{\gamma}_2^T\underline{v} \\ y\underline{\gamma}_2^T\underline{v} + \underline{\gamma}_3^T\underline{w} \\ z\underline{\gamma}_3^T\underline{w} + \underline{\gamma}_1^T\underline{u} \end{bmatrix}$$

or

(A-23)
$$\begin{aligned} \lambda_1 &= x\ a + b & a &= -K_r\underline{\gamma}_1^T\underline{u} \\ \lambda_2 &= y\ b + c \quad ; & b &= -K_r\underline{\gamma}_2^T\underline{v} \\ \lambda_3 &= z\ c + a & c &= -K_r\underline{\gamma}_3^T\underline{w} \end{aligned}$$

Solve (A-20) for x, y, and z and substitute into (A-23). The result is

(A-24)
$$\begin{aligned} \lambda_1^2 &= -a\lambda_3 + b\lambda_1 \\ \lambda_2^2 &= -b\lambda_1 + c\lambda_2 \\ \lambda_3^2 &= -c\lambda_2 + a\lambda_3 \end{aligned}$$

Adding these three equations gives

$$\lambda_1^2 + \lambda_2^2 + \lambda_3^2 = 0$$

and since λ_1, λ_2, and λ_3 are real, it follows that

(A-25)
$$\underline{\lambda} = 0$$

We return now to the case where elements of D are zero. If a single element, say $(R_1 h_3)_1$, is zero then Equation (A-4) is not satisfied and the associated determinants are non-zero. The matrix of the equations of the first three rows of D can be inverted to yield

$$\underline{\lambda} = 0$$

in accord with (A-25).

A colinear condition of two or three of the angular momentum vectors produces zeros in D. Suppose

$$\underline{h}_1 = \pm h_3$$

Then, since

$$R_1 \underline{h}_1 = 0$$

it follows that

(A-26) $$R_1 \underline{h}_3 = 0$$

and similarly

(A-27) $$R_3 \underline{h}_3 = R_3 \underline{h}_1 = 0$$

Substituting (A-26) and (A-27) into (4) gives

$$\underline{\delta} = \begin{bmatrix} R_1 \underline{h}_2 & 0 & 0 \\ R_2 \underline{h}_1 & R_2 \underline{h}_3 & 0 \\ 0 & R_3 \underline{h}_2 & 0 \end{bmatrix} \begin{pmatrix} \lambda_1 \\ \lambda_2 \\ \lambda_3 \end{pmatrix} = 0$$

from which it follows that

$$\lambda_1 = \lambda_2 = 0$$

Substituting (A-26) and (A-27) into (5) gives

$$\lambda_3 = 0$$

If all three angular momentum vectors are colinear, then all elements of D are zero and

$$\underline{\lambda} = 0$$

follows directly from (5).

The hypothesis $\underline{\lambda} \neq 0$ has resulted in a contradiction. There are no finite values of $\underline{\lambda}$ that produce equilibrium and $\underline{\lambda} = 0$ is therefore the necessary condition for equilibrium.

Appendix B

Relationship of Gimbal Angles to (α,ϕ,ψ) and $\underline{h}$

In Fig. 1 the Skylab CMG configuration is shown with the gyro momentum vectors $\underline{h}_1,\underline{h}_2$ and $\underline{h}_3$ aligned along vehicle (geometric) axes (x_v,y_v,z_v). The symmetrical* gimbal angles $\underline{\delta}$ $(\delta_1,\ldots,\delta_6)^T$ used here are related by Eq. (1) to the physical gimbal angles with defining directions shown in Fig. 1. Since the physical angles are related to $(\underline{h}_1,\underline{h}_2,\underline{h}_3)$ by**

$$(B\text{-}1)\quad \underline{h}_1^v = \begin{Bmatrix} c\hat{\delta}_1 c\hat{\delta}_2 \\ -c\hat{\delta}_1 s\hat{\delta}_2 \\ -s\hat{\delta}_1 \end{Bmatrix} \qquad \underline{h}_2^v = \begin{Bmatrix} -s\hat{\delta}_3 \\ c\hat{\delta}_3 c\hat{\delta}_4 \\ -c\hat{\delta}_3 s\hat{\delta}_4 \end{Bmatrix} \qquad \underline{h}_3^v = \begin{Bmatrix} -c\hat{\delta}_5 s\hat{\delta}_6 \\ -s\hat{\delta}_5 \\ c\hat{\delta}_5 c\hat{\delta}_6 \end{Bmatrix}$$

$\underline{\delta}$ can be written as

$$(B\text{-}2)\quad \underline{\delta} = \begin{Bmatrix} \delta_1 \\ \delta_2 \\ \delta_3 \\ \delta_4 \\ \delta_5 \\ \delta_6 \end{Bmatrix} = \begin{Bmatrix} -\sin^{-1}(h_{1z}) \\ \tan^{-1}(-h_{1y}/h_{1x}) \; -45° \\ -\sin^{-1}(h_{2x}) \\ \tan^{-1}(-h_{2z}/h_{2y}) \; -45° \\ -\sin^{-1}(h_{3y}) \\ \tan^{-1}(-h_{3x}/h_{3z}) \; -45° \end{Bmatrix}$$

It remains now to express $\underline{h}_1^v$, $\underline{h}_2^v$ and $\underline{h}_3^v$ in terms of (α,ϕ,ψ) and $\underline{h}$. First we describe the orientation of $\underline{h}$ as shown in Fig. (B-1a) by the angles L and ℓ. Thus

---

*i.e., relative to gimbal angle stops.

**Superscripts on vectors are used to emphasize the coordinate system in which its components are expressed.

$$\underline{h}^v = \begin{Bmatrix} h_x \\ h_y \\ h_z \end{Bmatrix} = \begin{Bmatrix} cLc\ell \\ sL \\ -cLs\ell \end{Bmatrix} \tag{B-3}$$

or

$$L = \sin^{-1}(h_y) \qquad 0 < |L| \leq 90° \tag{B-4}$$

$$\ell = \tan^{-1}(-h_z/h_x) \qquad 0 \leq |\ell| \leq 180° \tag{B-5}$$

Next consider the right-handed coordinate system (x_h, y_h, z_h) shown in Fig. (B-1a) where x_h is along $\underline{h}$ and z_h is in the (y_v, z_v) plane. The coordinate transformation relative to (x_v, y_v, z_v) is

$$\begin{Bmatrix} x_h \\ y_h \\ z_h \end{Bmatrix} = A \begin{Bmatrix} x_v \\ y_v \\ z_v \end{Bmatrix} \tag{B-6}$$

where

$$A = [L]_z [\ell]_y \tag{B-7}$$

Now let $\underline{h}_1$ be displaced from $\underline{h}$ by α* and rotated about $\underline{h}$ by ϕ as illustrated in Fig. (B-1b). Note that $\phi = 0$ is referenced to the (x_h, y_v) plane. Thus,

$$\underline{h}_1^h = B^T \begin{Bmatrix} 1 \\ 0 \\ 0 \end{Bmatrix} \tag{B-8}$$

where

$$B = [-\alpha]_z [-\phi]_x \tag{B-9}$$

---

*See Footnote *, p. 13.

or using Eq. (B-6) we get

$$\underline{h}_1^v = A^T \underline{h}_1^h = A^T B^T \begin{Bmatrix} 1 \\ 0 \\ 0 \end{Bmatrix} \tag{B-10}$$

As shown in Fig. (B-1b), $\underline{h}_{23} = \underline{h}_2 + \underline{h}_3$ is displaced from $\underline{h}$ by γ and diametrically opposite to $\underline{h}_1$. Now let $\underline{h}_2$ and $\underline{h}_3$ be displaced by β from $\underline{h}_{23}$ and rotated about $\underline{h}_{23}$ by ψ as in Fig. (B-1c). This gives*

$$\underline{h}_2^h = \left[[-\beta]_z [\psi]_x [\gamma]_z [-\phi]_x \right]^T \begin{Bmatrix} 1 \\ 0 \\ 0 \end{Bmatrix} = C^T \begin{Bmatrix} c\beta \\ -s\beta \\ 0 \end{Bmatrix} \tag{B-11}$$

$$\underline{h}_3^h = \left[[\beta]_z [\psi]_x [\gamma]_z [-\phi]_x \right]^T \begin{Bmatrix} 1 \\ 0 \\ 0 \end{Bmatrix} = C^T \begin{Bmatrix} c\beta \\ s\beta \\ 0 \end{Bmatrix} \tag{B-12}$$

where

$$C \equiv [\psi]_x [\gamma]_z [-\phi]_x \tag{B-13}$$

Note that $\psi=0$ is referenced to the plane formed by $\underline{h}_{23}$ and $\underline{h}$. Using Eq. (B-6) we get

$$\underline{h}_2^v = A^T \underline{h}_2^h = A^T C^T \begin{Bmatrix} c\beta \\ -s\beta \\ 0 \end{Bmatrix} \tag{B-14}$$

and

$$\underline{h}_3^v = A^T \underline{h}_3^h = A^T C^T \begin{Bmatrix} c\beta \\ s\beta \\ 0 \end{Bmatrix} \tag{B-15}$$

---

*While this formulation is written to evaluate $\underline{h}_1^v, \underline{h}_2^v$ and $\underline{h}_3^v$ given H, $\underline{h}$ and (α, ϕ, ψ) it also possible to evaluate (α, ϕ, ψ) given $(\underline{h}_1^v, \underline{h}_2^v, \underline{h}_3^v)$ with a few simple manipulations of Eqs. (B-8)-(B-13).

The results in Eqs. (B-8), (B-12) and (B-13) apply to 3 CMGs. For 2 CMGs certain modifications are needed in order to use the above equations. These are tabulated in Table B-1.

TABLE B-1 PARAMETER MODIFICATIONS FOR 2 CMG s

APPLICABLE CMG PAIR	B	C	β	a
$\underline{h}_1$ & $\underline{h}_2$	$[-a]_z\ [-\phi]_x$	$[a]_z\ [-\phi]_x$	0	$\cos^{-1}(H/2)$
$\underline{h}_1$ & $\underline{h}_3$	$[-a]_z\ [-\phi]_x$	$[a]_z\ [-\phi]_x$	0	
$\underline{h}_2$ & $\underline{h}_3$	$[-\phi]_x$	$[-\phi]_x$	a	

An analytical evaluation of $\underline{\delta}$ from Eqs. (B-2) and (B-7)-(B-13) is not very rewarding except for a few special cases. Nevertheless this formulation is well suited for machine computation and systematic scanning of the total gimbal angle space.

Appendix C

A Dynamic Origin Approach for 2 and 3 CMGs

The method outlined here is based on the geometry in Fig.(C-1a) which shows the relative orientation of $\underline{h}$ and a unit vector $\underline{e}_k$ parallel to the outer gimbal axis of CMG k (k=1,2,3)*. The dashed curve (C) represents the possible location of its unit angular momentum vector $\underline{h}_k$ for an angle α_k between $\underline{h}$ and $\underline{h}_k$. If, for instance, $\underline{h}_k$ is at point 1 on C, then

$$(C\text{-}1) \qquad \underline{\delta}_k = \begin{Bmatrix} \delta_{(2k-1)} \\ \delta_{(2k)} \end{Bmatrix} = \begin{Bmatrix} -\sigma \\ \delta_{p(2k)} + \xi \end{Bmatrix} \qquad k = 1,2,3$$

where $\delta_{p(2k)}$ is the outer gimbal angle component of $\underline{\delta}_p$ for CMG k.

From the discussion of equilibrium loci in Section 4 it is desirable to define a dynamic origin δ_N along a path which connects the pole and anti-pole in allowable gimbal angle space. A curve that satisfies this condition and simultaneously minimizes the inner gimbal angle excursion is the great circle B in Fig.(C-1a), which is normal to meridian A containing $\underline{e}_k$ and $\underline{h}$. The analytical formulation for this curve can be expressed in terms of α_k and ρ_k as

$$(C\text{-}2) \qquad s\delta_{(2k-1)} = -c\rho_k c\alpha_k$$

$$\tan(\delta_{(2k)} - \delta_{p(2k)}) = -\mu \tan \alpha_k / s\rho_k \qquad k=1,2,3$$

where

$$(C\text{-}3) \qquad \mu = \begin{cases} +1 & \delta_{p(2k)} \geq 0 \\ -1 & \delta_{p(2k)} < 0 \end{cases}$$

specifies the "useful half" of B,** hereafter called the normal trajectory (NT). Typical trajectories are shown in Fig.(C-1b).***

---

*Here $\underline{e}_k$ is defined along $+z_v$, $+x_v$ or $+y_v$ if k=1,2, or 3 respectively. See Fig.(1).

**This is the half circle of B not crossing the gimbal stops.

***The subscripts I and 0 are equivalent to (2k-1) and (2k) in Eq.(C-2).

2 CMGs

Because of the requirement that $\alpha_k = \alpha \equiv \cos^{-1}(H/2)$, the NTs for 2 CMGs are not always compatible for arbitrary $\underline{h}$. They are compatible however if $\underline{h}$ lies in the plane formed by the two outer gimbal axes (i.e. (x_v, z_v) for CMGs 1&2; (x_v, z_v) for CMGs 2&3; (y_v, x_v) for CMGs 3&1. If they are compatible, then defining the components of $\underline{\delta}_N$ according to Eq.(C-2) will result in a major $\underline{\delta}_E$ locus corresponding to the respective NTs, since $P(\underline{\delta})$ in Eq.(55) would be exactly zero along the NT. If they are not compatible, defining $\underline{\delta}_N$ according to Eq.(C-2) will result in a major $\underline{\delta}_E$ locus which minimizes the excursion from the NT. The $\underline{\delta}_E$ locus in Fig.(22) corresponding to $\underline{\delta}_N \neq 0$ is an example of this.

The major $\underline{\delta}_E$ locus with $\underline{\delta}_N$ defined this way could be computed from the procedure in Appendix B for 2 CMGs, if the optimal ϕ corresponding to minimizing $P(\underline{\delta})$ in Eq.(55) were known. A useful approximation for ϕ_{opt} given here without proof is

$$\phi_{opt} = (\phi_{Ni} + \phi_{Nj})/2 \tag{C-4}$$

where ϕ_{Ni} and ϕ_{Nj} represent the (minimum) rotation of the respective NTs for CMGs i and j about $\underline{h}$ such that they are coplanar and thus form a compatible trajectory. Expressions for tan ϕ_{Nk} (k=1,2,3) are given in Table (C-1).

TABLE C-1

TAN ϕ_{Nk}*

CMG (k) \ CMG PAIR	1 & 2	2 & 3	3 & 1
1**	$\frac{-\mu S\ell SL}{-\mu C\ell}$		
2**	$\frac{-\mu C\ell SL}{\mu S\ell}$		$\frac{\mu C\ell SL}{-\mu S\ell}$
3		$\mu\infty$	

* $\mu = +1\ (\delta_{p(2k)} > 0)$; $\mu = -1\ (\delta_{p(2k)} < 0)$

**ALGEBRAIC SIGNS OF NUMERATOR AND DENOMINATOR TERMS SPECIFY THE QUADRANT FOR ϕ_{Nk}

3 CMGs

Here we note that the NTs are always compatible for 3 CMGs so that the dynamic origin approach with $\underline{\delta}_N$ defined according to Eq.(C-2) might also be applied in that case. The compatibility can be observed after resolving the unit vectors $\underline{h}_k$ into components along $\underline{h}$ such that

$$\underline{h}_k = c\alpha_k \underline{h} + s\alpha_k \underline{h}_{nk} \tag{C-5}$$

where

$$\underline{h}_{nk} \equiv \tilde{\underline{h}}\underline{e}_k / s\rho_k \tag{C-6}$$

Thus,

$$\underline{h}_t = H\underline{h} = \sum_{k=1}^{3} \underline{h}_k = \sum_{k=1}^{3} c\alpha_k \underline{h} + \sum_{k=1}^{3} \tilde{\underline{h}}\underline{e}_k \, s\alpha_k / s\rho_k \tag{C-7}$$

and since

$$H = c\alpha_1 + c\alpha_2 + c\alpha_3 \tag{C-8}$$

it follows that

$$\underline{0} = \sum_{k=1}^{3} \tilde{\underline{h}}\underline{e}_k \, s\alpha_k / s\rho_k \tag{C-9}$$

Substituting for $\underline{e}_k$* and $\underline{h} = (h_x \; h_y \; h_z)^T$ yields

$$\begin{Bmatrix} 0 \\ 0 \\ 0 \end{Bmatrix} = \frac{s\alpha_1}{s\rho_1} \begin{Bmatrix} h_y \\ -h_x \\ 0 \end{Bmatrix} + \frac{s\alpha_2}{s\rho_2} \begin{Bmatrix} 0 \\ h_z \\ -h_y \end{Bmatrix} + \frac{s\alpha_3}{s\rho_3} \begin{Bmatrix} -h_z \\ 0 \\ h_x \end{Bmatrix} \tag{C-10}$$

where ρ_1, ρ_2, and ρ_3 are defined by Eq.(50). Thus given $\underline{h}$ and H Eqs.(C-8) and (C-10) can be solved to find the corresponding CMG distribution (α_1, α_2, α_3) about $\underline{h}$, although in general this is not unique for H<1.

*See Footnote ** on p.C-1.

Appendix D

List of Symbols

This list defines major symbols appearing in two or more sections. Minor symbols or symbols appearing in only one section are omitted.

Greek Symbols	Definition
α or α_ℓ	angle between $\underline{h}_\ell$ and $\underline{h}$ (ℓ=1,2,3)
α_{max}	maximum α possible for a given H
$\underline{\delta}$	vector (6x1) of symmetrical* gimbal angles, $(\delta_1 \ldots \delta_6)^T$
$\dot{\underline{\delta}}$	$d\underline{\delta}/dt$
$\underline{\delta}_E$	$\underline{\delta}$ at equilibrium ($\dot{\underline{\delta}}=\underline{0}$)
$\underline{\delta}_\ell$	vector (2x1) of symmetrical* gimbal angles for CMG ℓ (ℓ=1,2,3)
$\underline{\delta}_N$	vector (6x1) of symmetrical* gimbal angles defining dynamic origin
$\underline{\delta}_p$	$\underline{\delta}$ at CMG saturation (H=3 or H=2) for a given $\underline{h}$
δ_{pI}	an inner gimbal angle component of $\underline{\delta}_p$ (I=1,3,5)
δ_{pO}	an outer gimbal angle component of $\underline{\delta}_p$ (O=2,4,6)
η_x	minimum angle between sunline and orbital plane (see Footnote*, p.19)
$\underline{\lambda}$	vector (3x1) in CMG rotation law defined by $-K_R D^T Q \underline{\delta}$
ρ_ℓ	angle between $\underline{e}_\ell$ and $\underline{h}$
ϕ	rotation of total CMG momentum configuration about $\underline{h}$
$\underline{\phi}$	vector (3x1) of rotation angles $(\phi_{12}, \phi_{23}, \phi_{31})$ about respective CMG pairs
$\dot{\underline{\phi}}$	$d\underline{\phi}/dt$
$\underline{\psi}$	rotation of $\underline{h}_j$ and $\underline{h}_k$ about their sum $(\underline{h}_j+\underline{h}_k)$
$\underline{\omega}$	spacecraft angular velocity
English Symbols	
D	matrix (6x3) with elements $\underline{R}_i\underline{h}_j$ (i,j=1,2,3; Note: $\underline{R}_i\underline{h}_i=\underline{0}$)

*relative to gimbal stops

English Symbols	Definitions
$\underline{e}_\ell$	vector (3x1) parallel to outer gimbal axis of CMG ℓ: $\underline{e}_1 = \begin{Bmatrix} 0 \\ 0 \\ 0 \end{Bmatrix}$, $\underline{e}_2 = \begin{Bmatrix} 1 \\ 0 \\ 0 \end{Bmatrix}$, $\underline{e}_3 = \begin{Bmatrix} 0 \\ 1 \\ 0 \end{Bmatrix}$
$\underline{h}$	unit vector (3x1) specifying the direction of $\underline{h}_t$
H	scalar specifying the magnitude of $\underline{h}_t$ $\begin{cases} 0 \leq H \leq 3 & 3 \text{ CMGs} \\ 0 \leq H \leq 2 & 2 \text{ CMGs} \end{cases}$
H_{12}, H_{23}, H_{31}	magnitudes corresponding to the sum of 2 CMG unit momentum vectors
$\underline{h}_\ell$	unit angular momentum vector (3x1) for CMG ℓ (ℓ=1,2,3)
$\underline{h}_t$	vector (3x1) representing total CMG angular momentum (normalized to spin angular momentum of one CMG.)
K_R	rotation law gain constant
ℓ	angle (longitude) between the projection of $\underline{h}$ in (x_v, z_v) plane and x_v
L	angle (latitude) between $\underline{h}$ and (x_v, z_v) plane
$P(\underline{\delta})$	performance function of gimbal angles; quadratic form: $\frac{1}{2}\underline{\delta}^T Q \underline{\delta}$
Q	rotation law weighting matrix (6x6); Q=diag (1,q,1,q,1,q)
R_1, R_2, R_3	matrix (2x3) transformation relating gimbal axes to vehicle axes for CMGs 1,2 and 3
SL	limit for elements of D^T in rotation law
(x_v, y_v, z_v)	Skylab geometric coordinate axes

Special Symbals	
⊕	point on gimbal angle map corresponding to the pole ($\underline{\delta}_p$)
⊖	point on gimbal angle map corresponding to the anti-pole (i.e. the $\underline{\delta}_p$ for $-\underline{h}$)
c( )	cos ( )
s( )	sin ( )
t( )	tan ( )
T	vector or matrix transpose operation

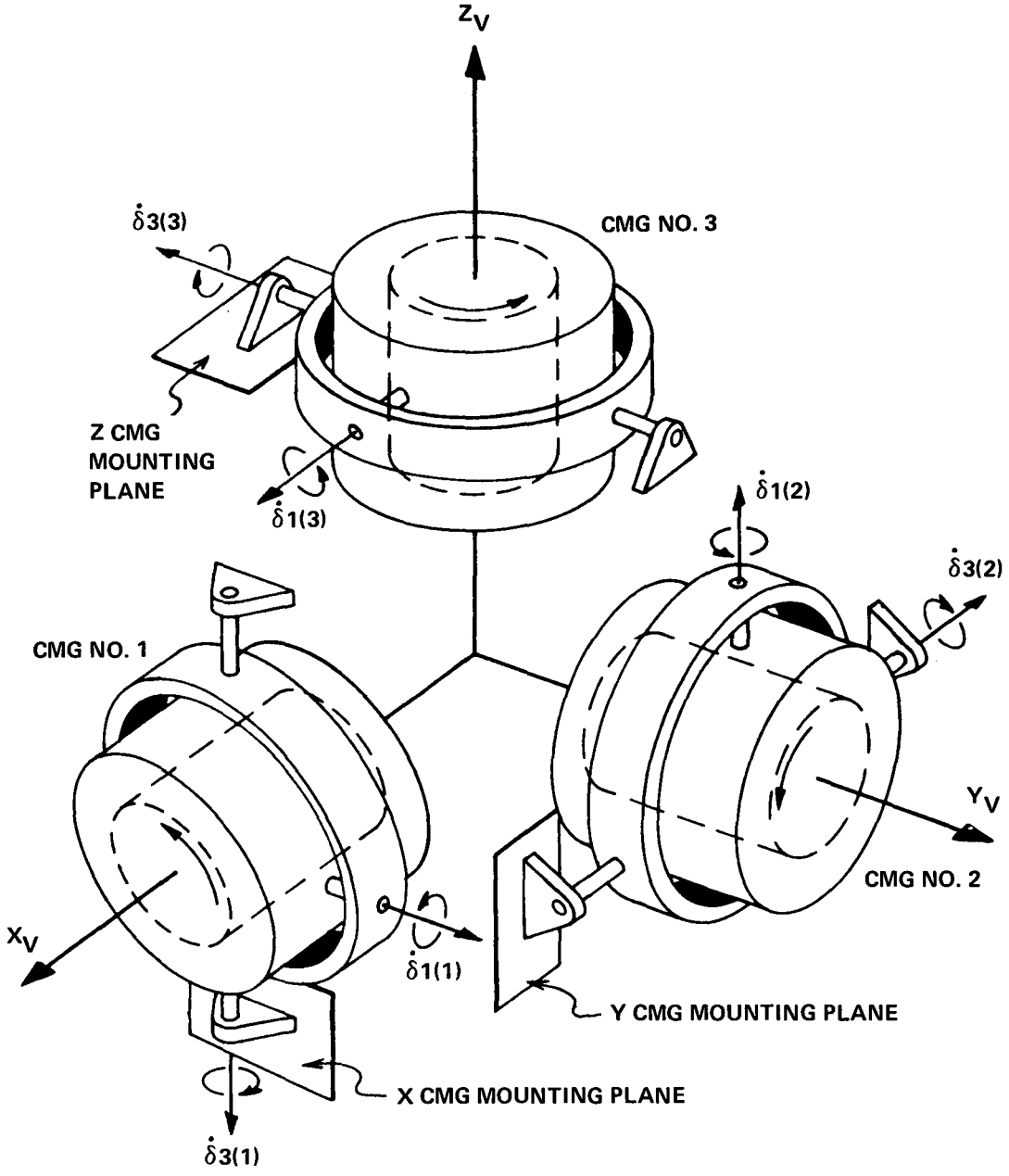

FIGURE 1 - SKYLAB CMG CONFIGURATION

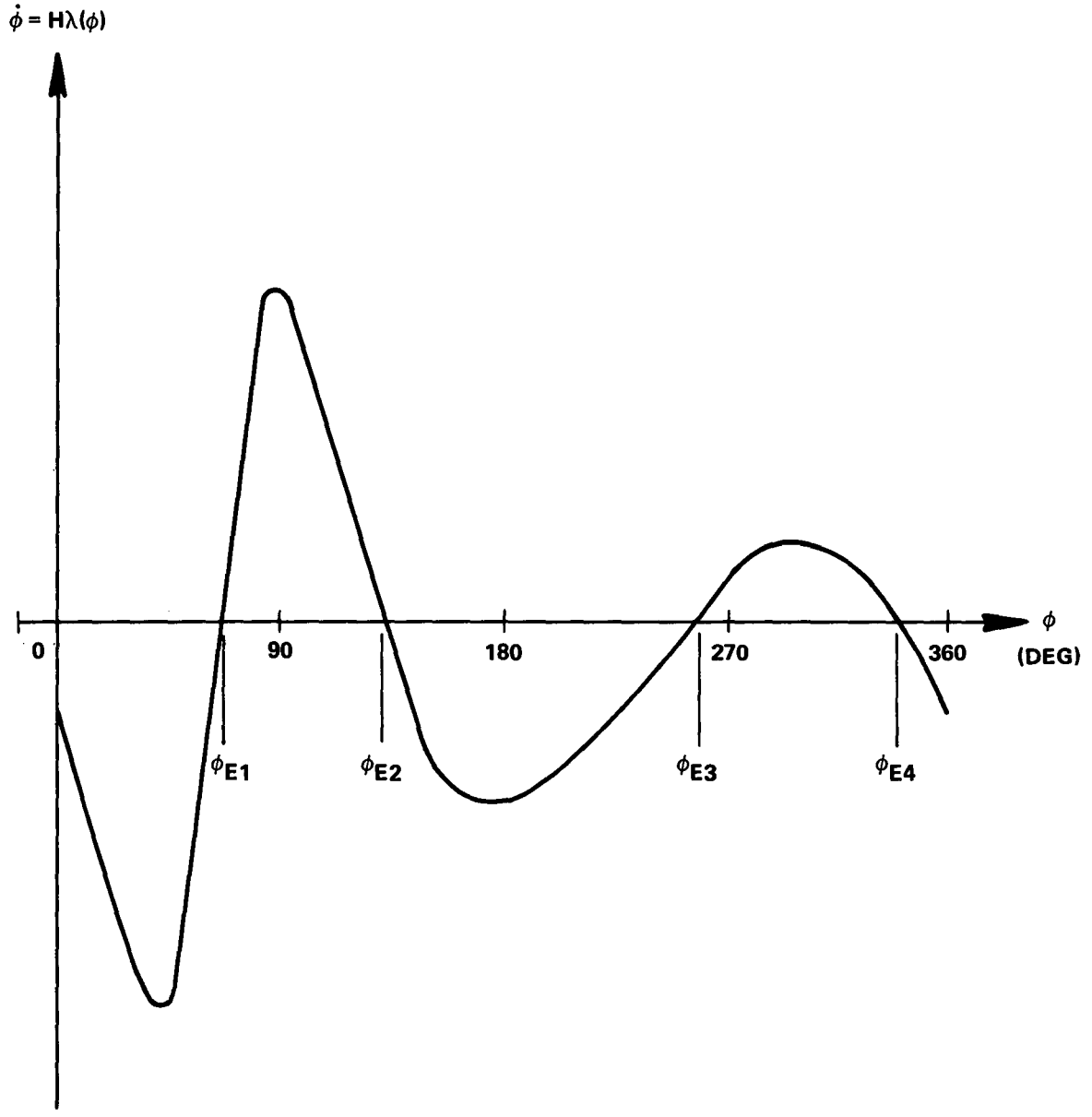

FIGURE 2 TWO CMG ROTATION LAW DYNAMICS ($\dot{\phi}$ vs ϕ)

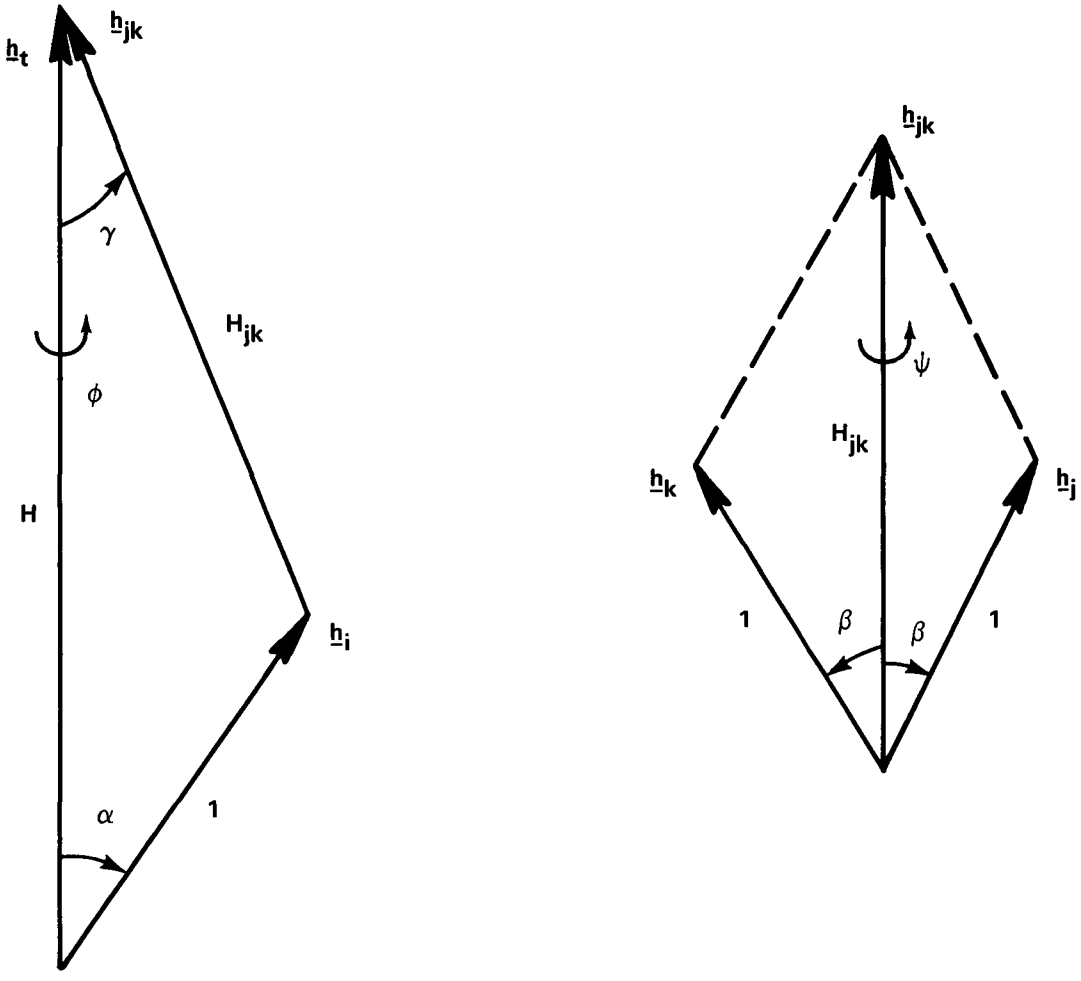

FIGURE 3 - GENERAL ORIENTATION OF CMG UNIT MOMENTUM VECTORS

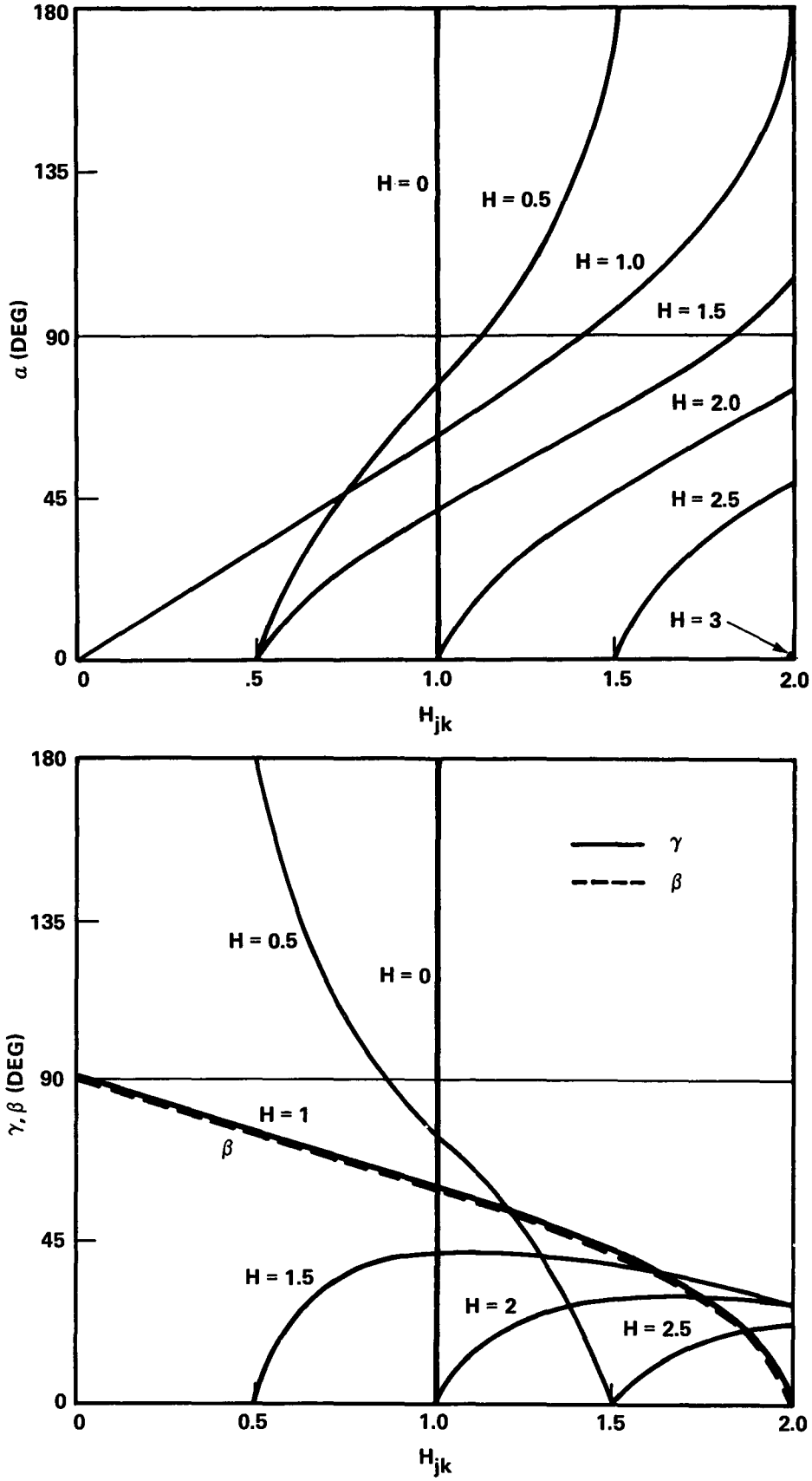

FIGURE 4 α, β, γ, vs H_{jk} FOR CONSTANT H

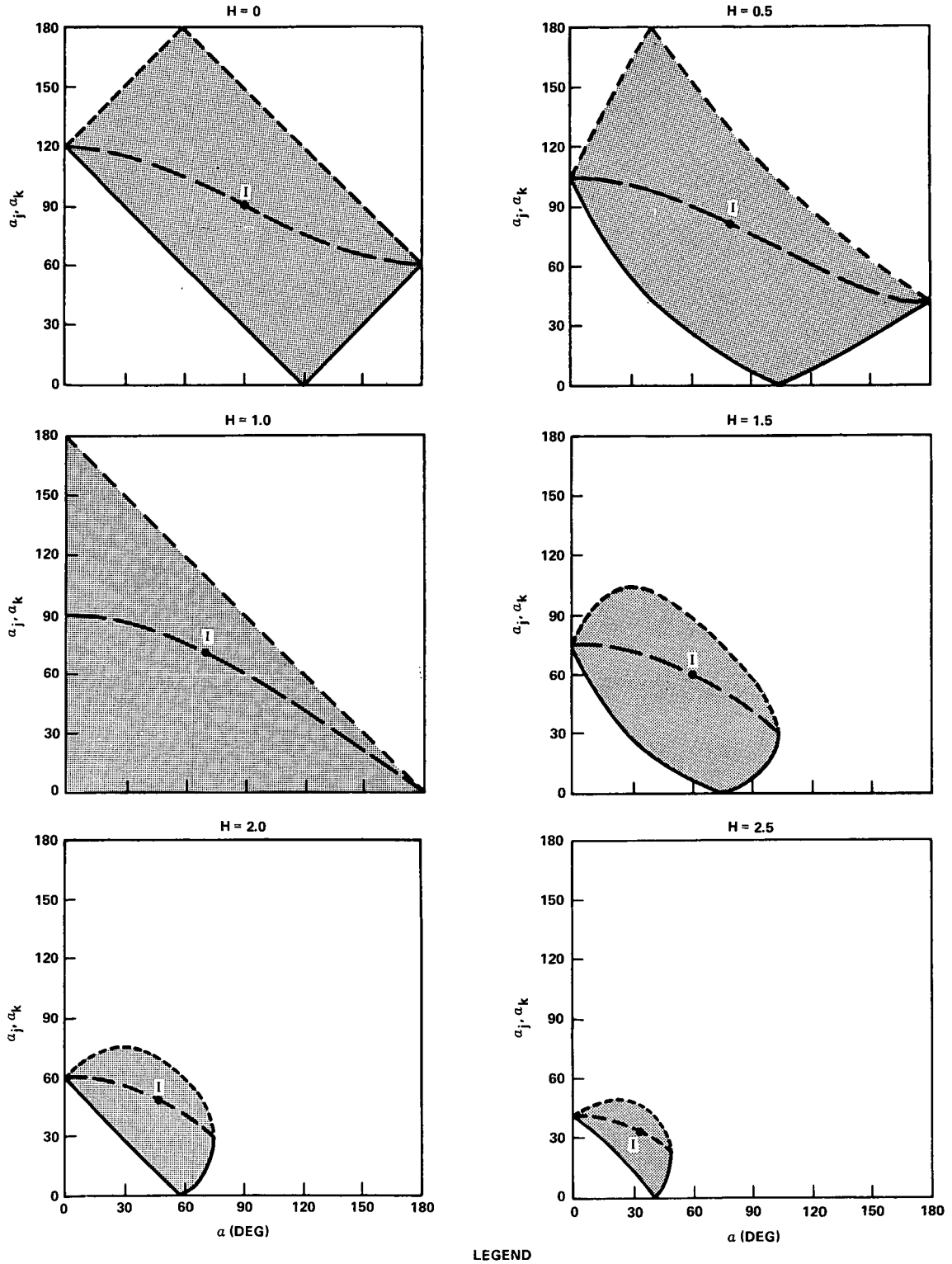

FIGURE 5 α_j, α_k vs α FOR CONSTANT H AND ψ

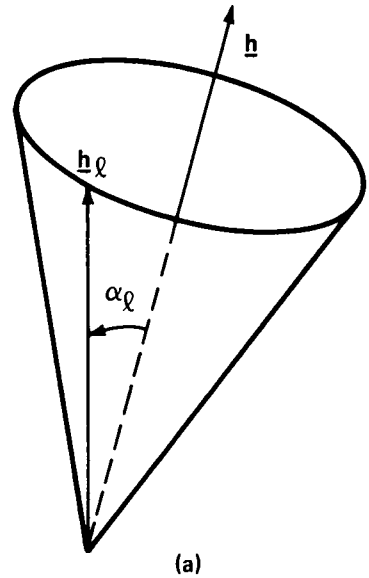

(a)

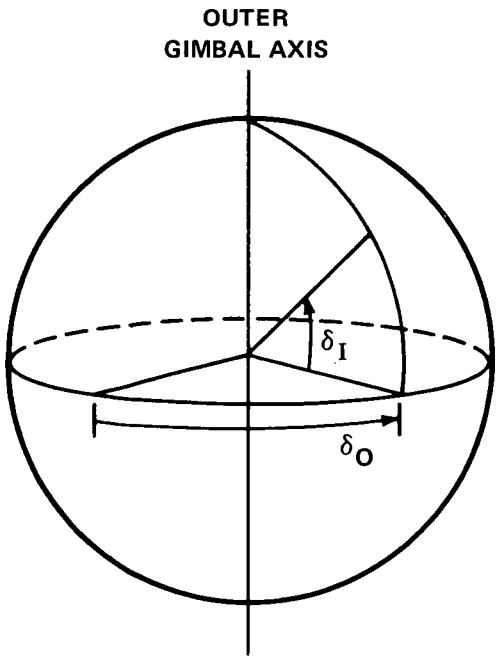

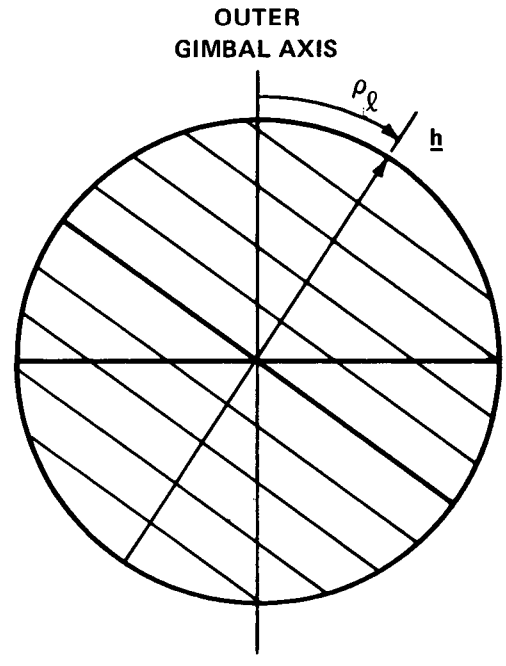

(b)

FIGURE 6 - GEOMETRY FOR CMG GIMBAL ANGLE MAPS

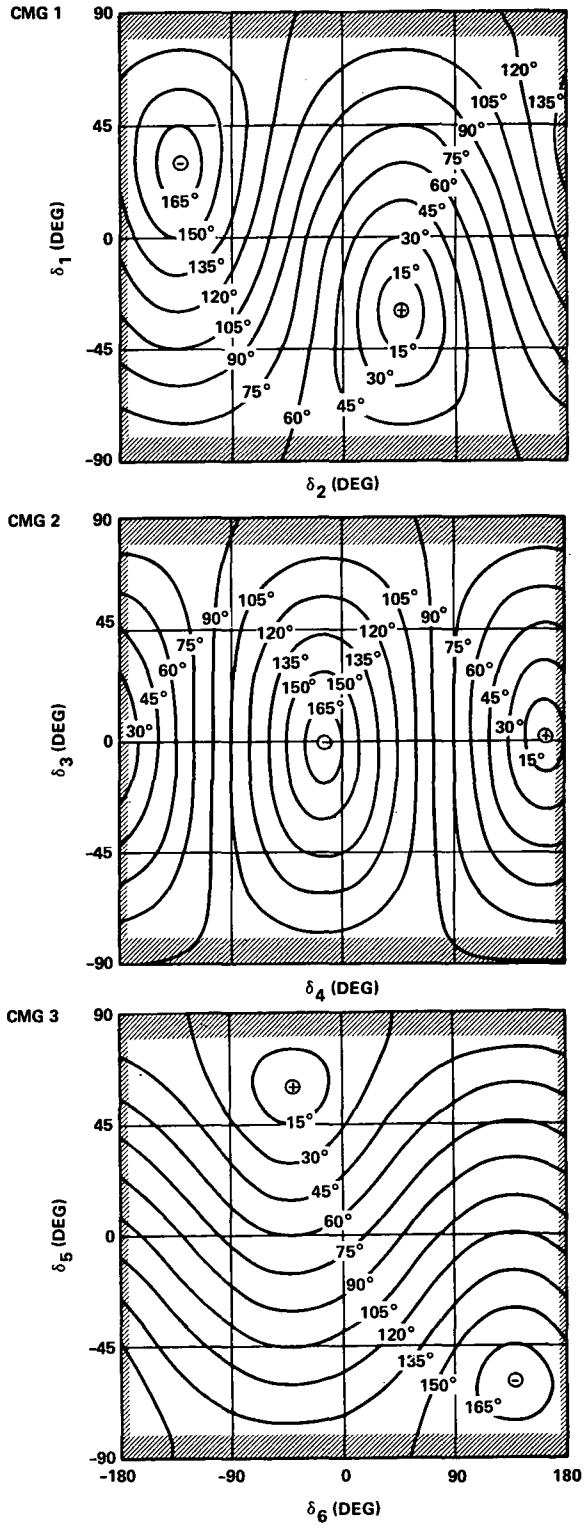

FIGURE 7 GIMBAL ANGLE MAPS FOR $\underline{h} = (0, -.866, .5)^T$

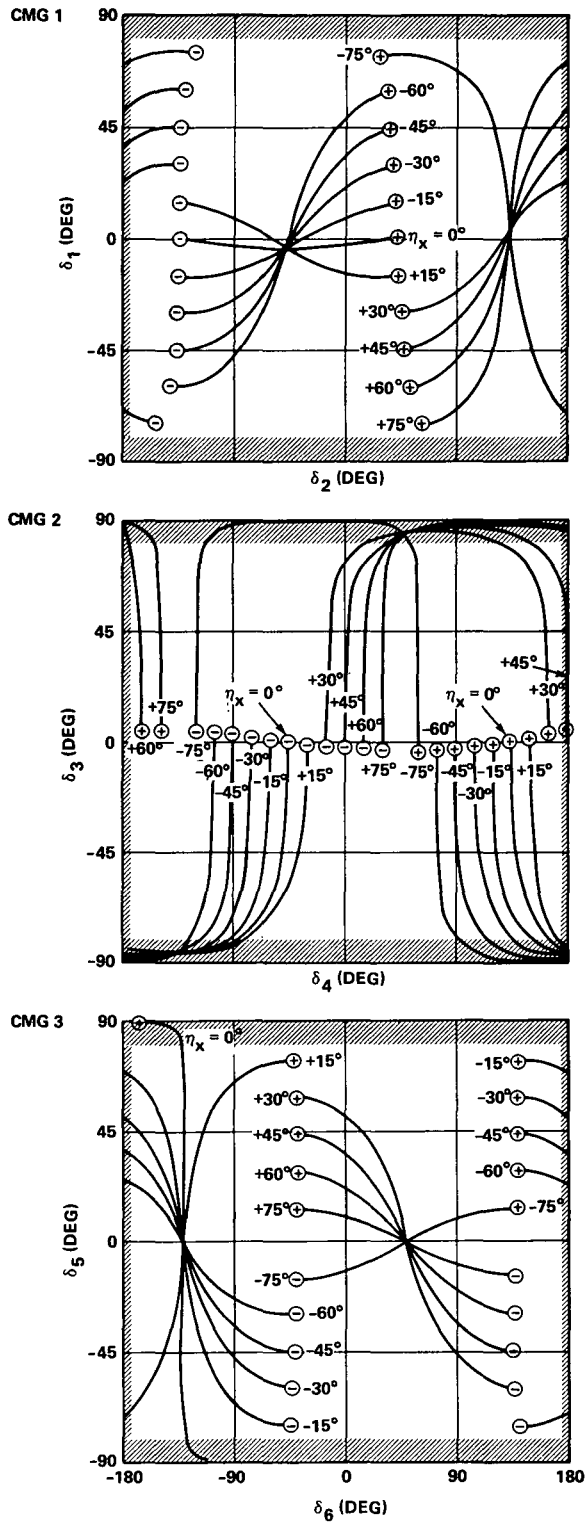

FIGURE 8 POLE MIGRATIONS IN THE SOLAR INERTIAL MODE vs η_x

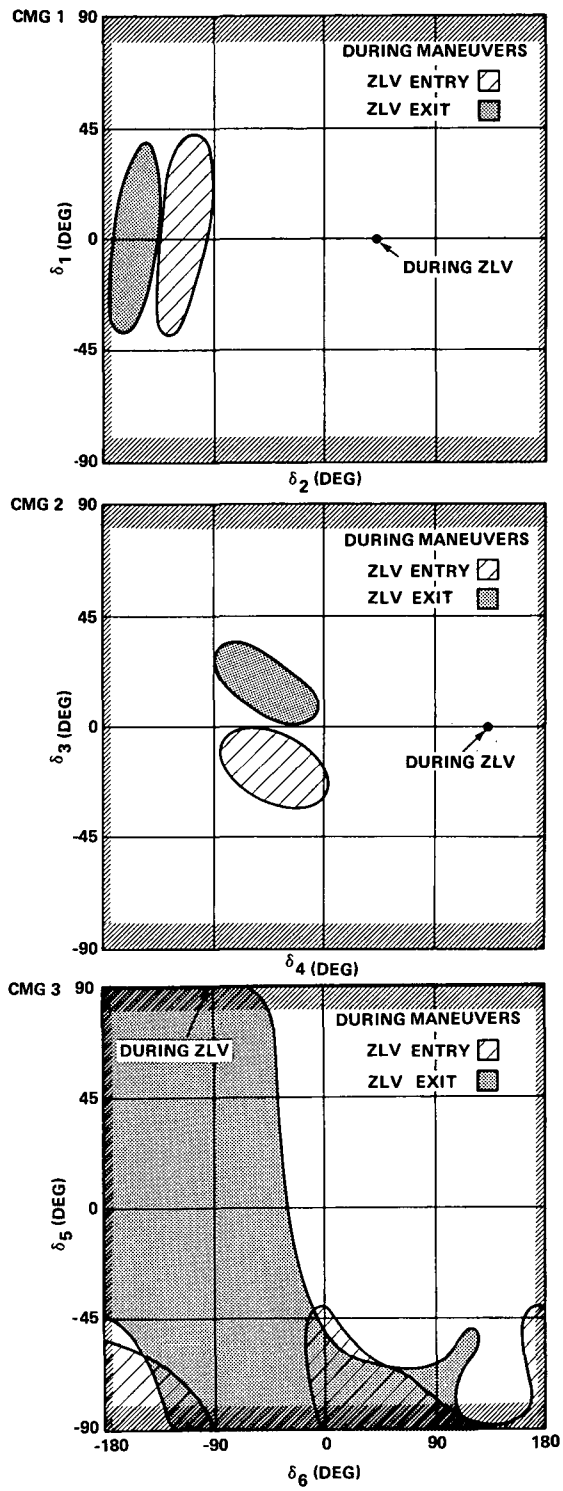

FIGURE 9 DOMINANT POLE LOCATIONS IN THE ZLV/XIOP MODE
(60° PASS CENTERED AT ORBITAL NOON)

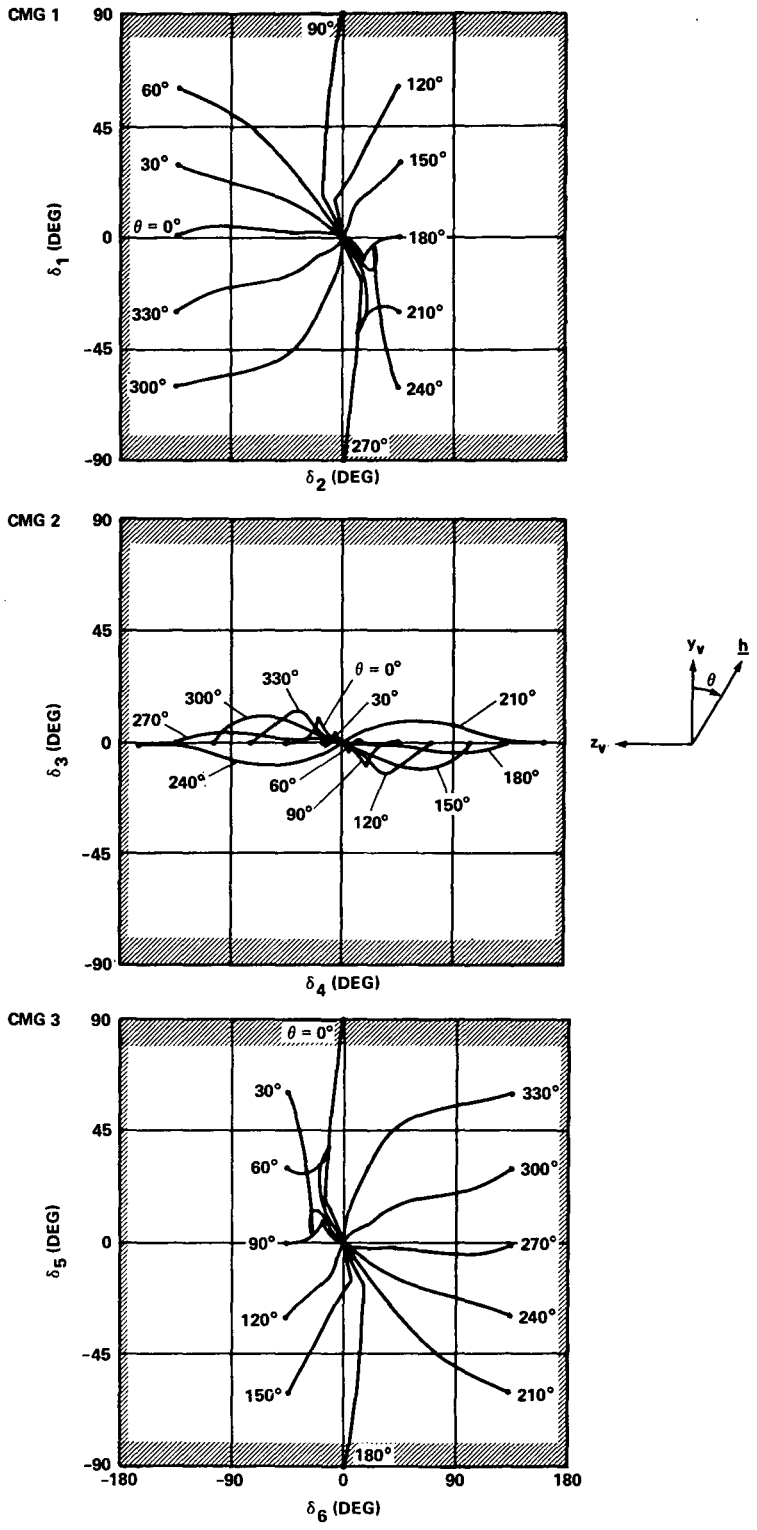

FIGURE 10 EQUILIBRIUM LOCI FOR 3 CMG s WITH $\underline{h}$ IN (y_v, z_v) PLANE

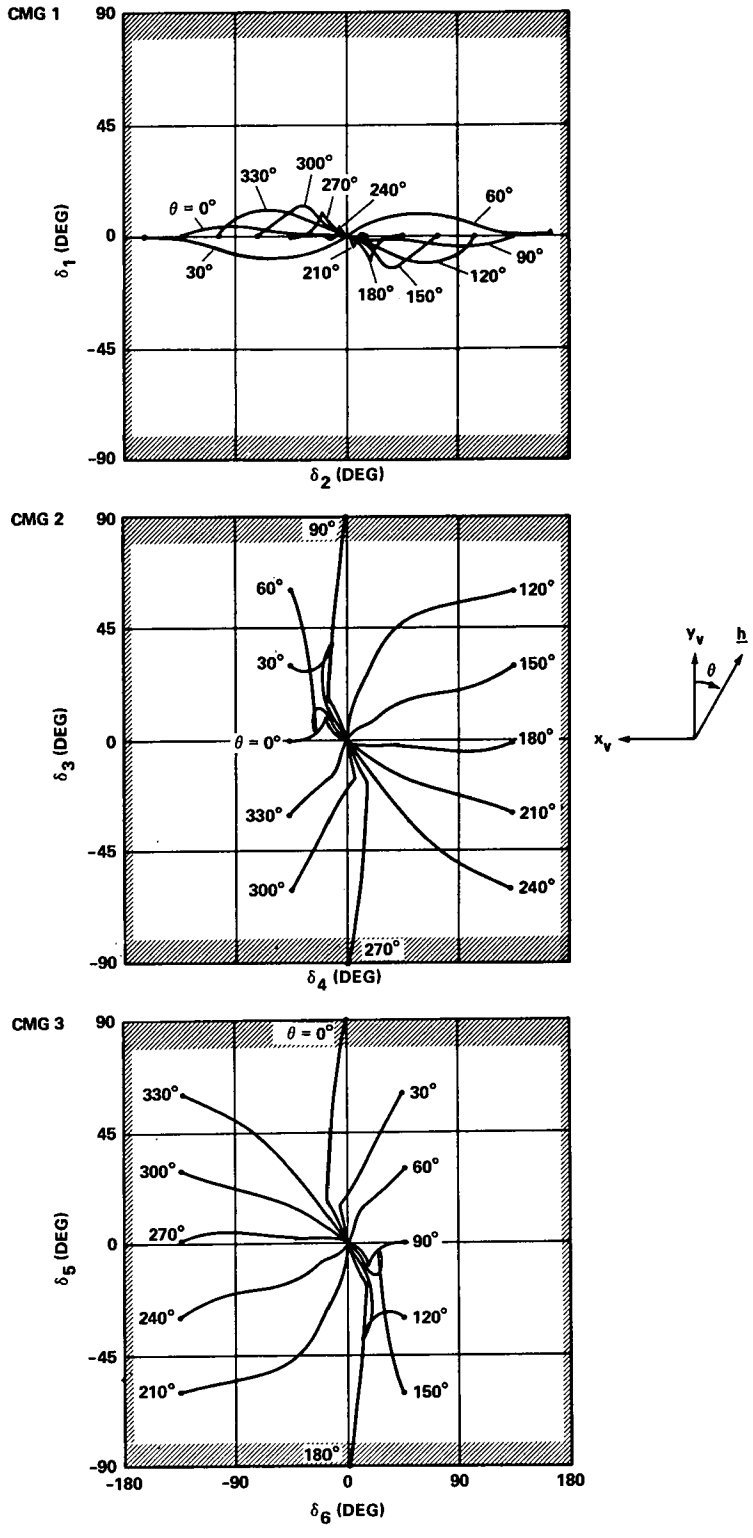

FIGURE 11 EQUILIBRIUM LOCI FOR 3 CMG s WITH $\underline{h}$ IN (x_v, y_v) PLANE

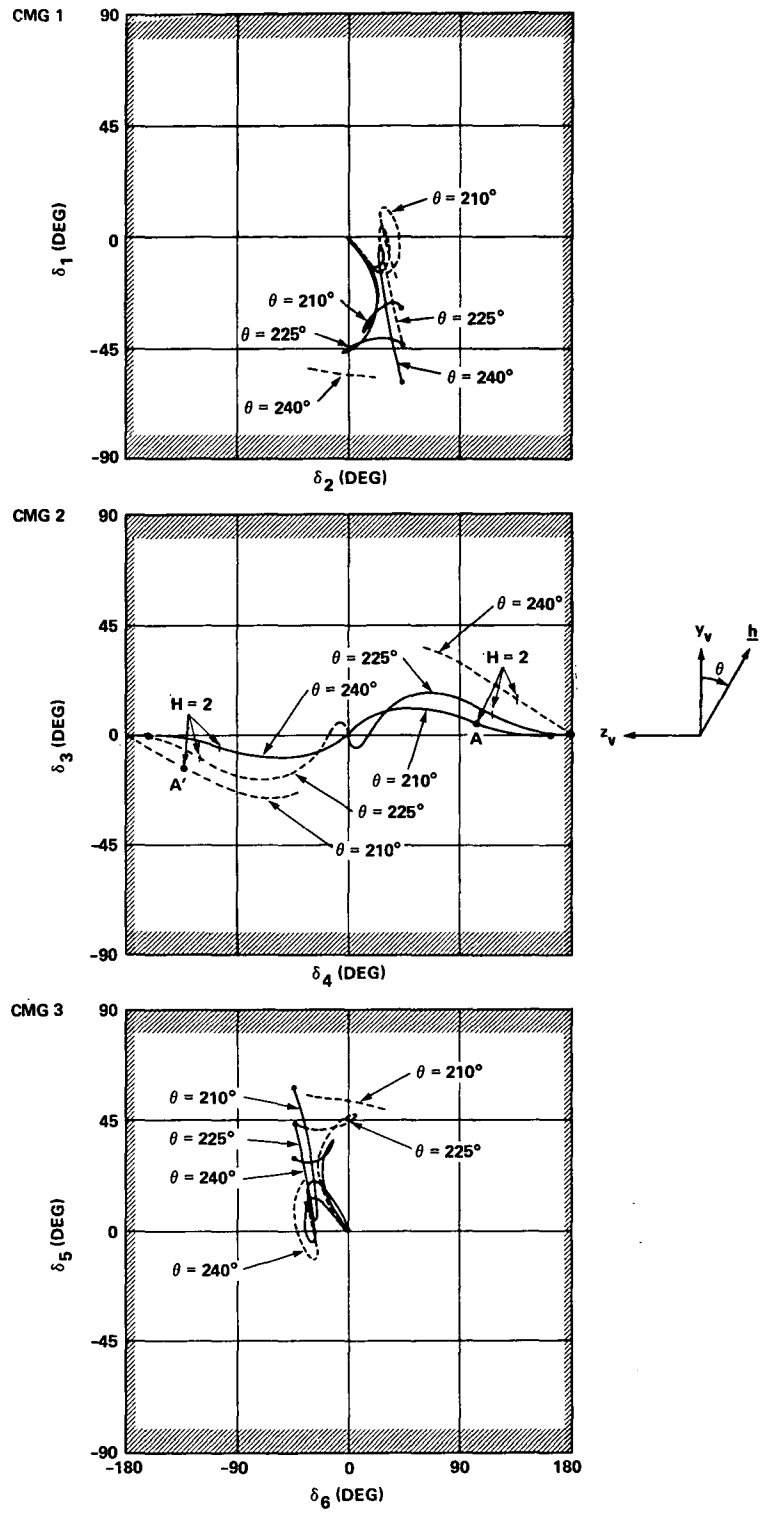

FIGURE 12 MULTIPLE EQUILIBRIUM LOCI FOR 3 CMG s WITH $\underline{h}$ IN (y_v, z_v) PLANE

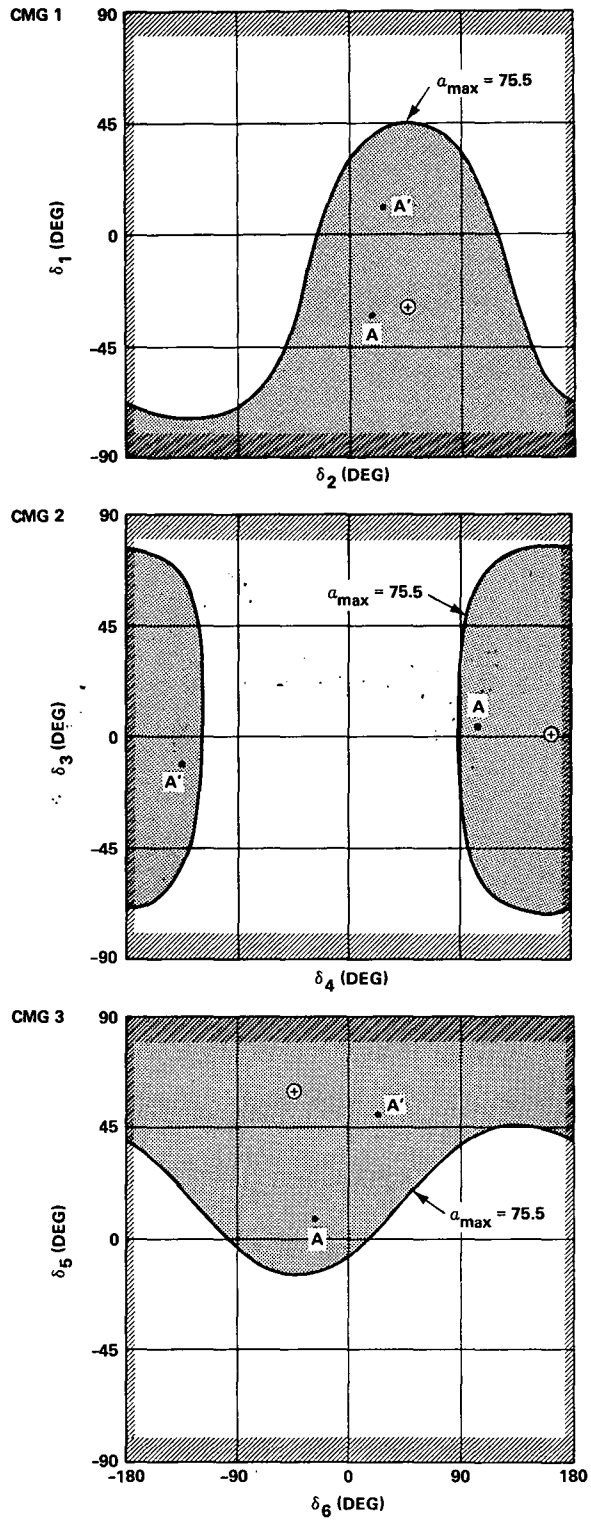

FIGURE 13 ALLOWABLE GIMBAL ANGLE SPACE FOR 3 CMG s AND LOCATION OF 2 STABLE EQUILIBRIA FOR $\underline{h} = (0, -.866, .5)^T$ AND H = 2

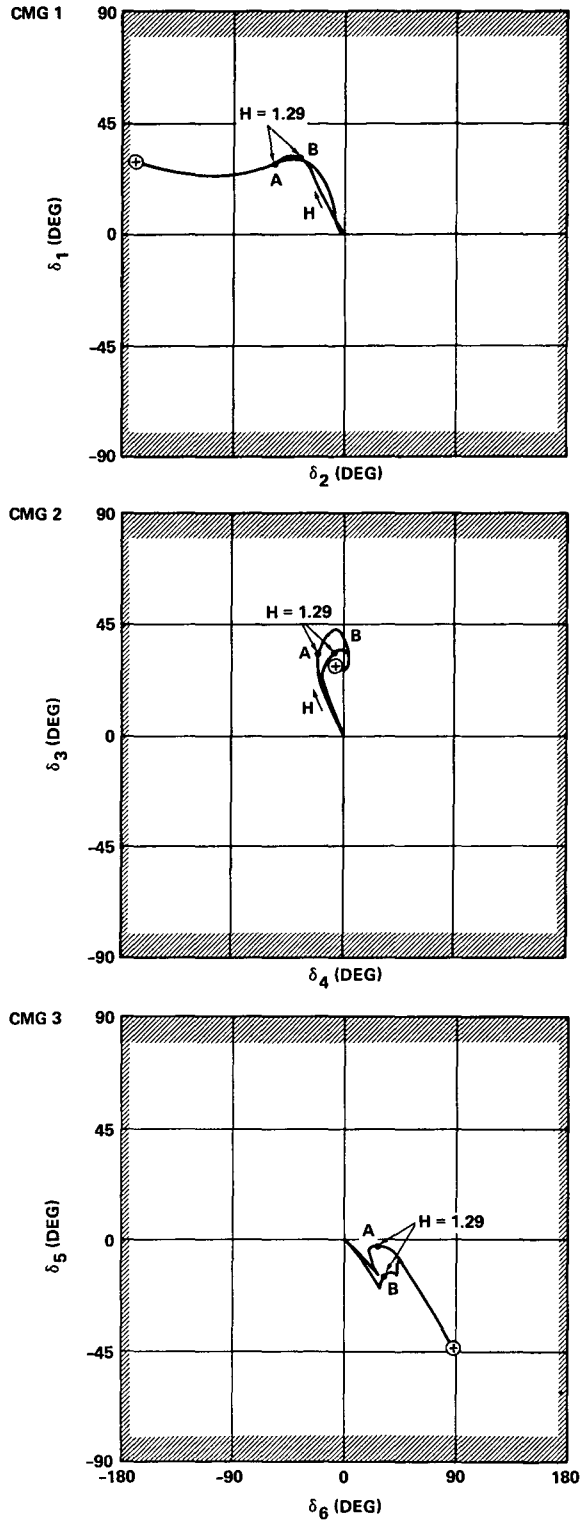

FIGURE 14 MULTIPLE EQUILIBRIA WITHOUT BIFURCATION FOR 3 CMG's AND $\underline{h} = (-.5, .707, -.5)^T$

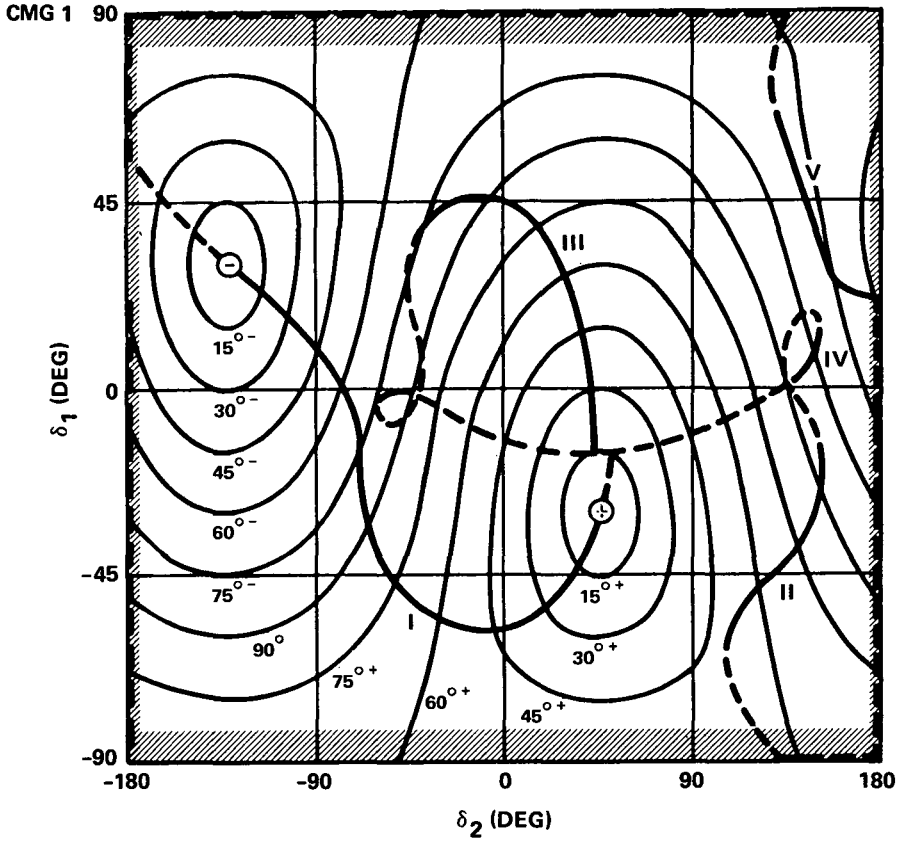

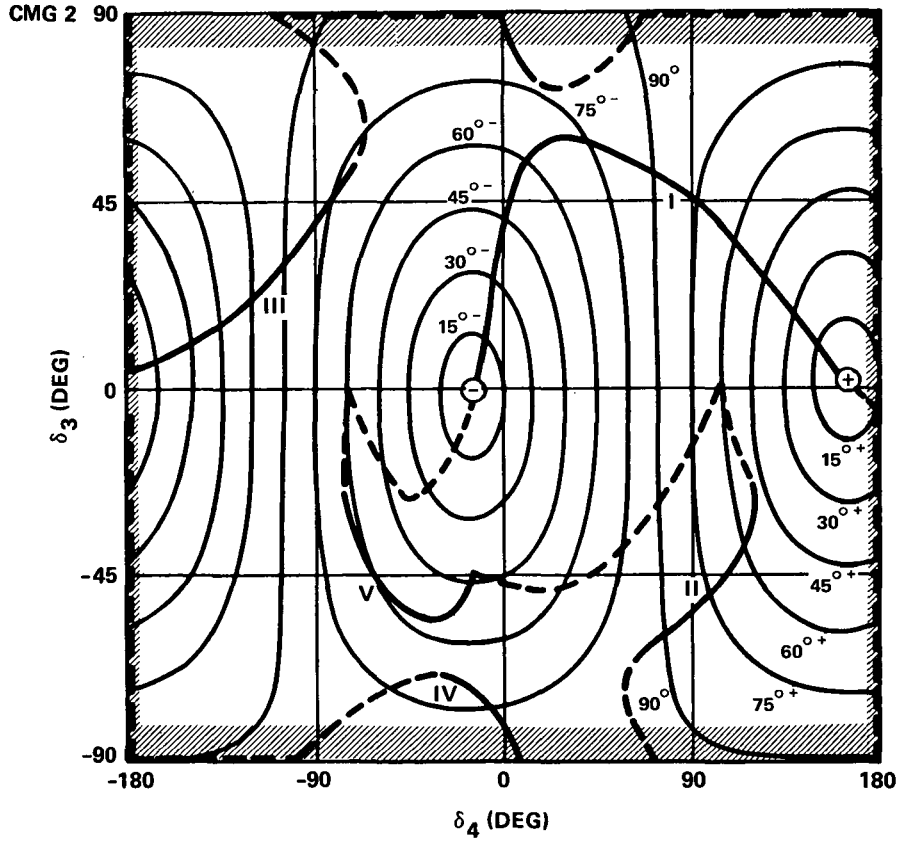

FIGURE 15 EQUILIBRIUM LOCI FOR CMG's 1 & 2 FOR $\underline{h} = \pm(0, -.866, .5)^T$

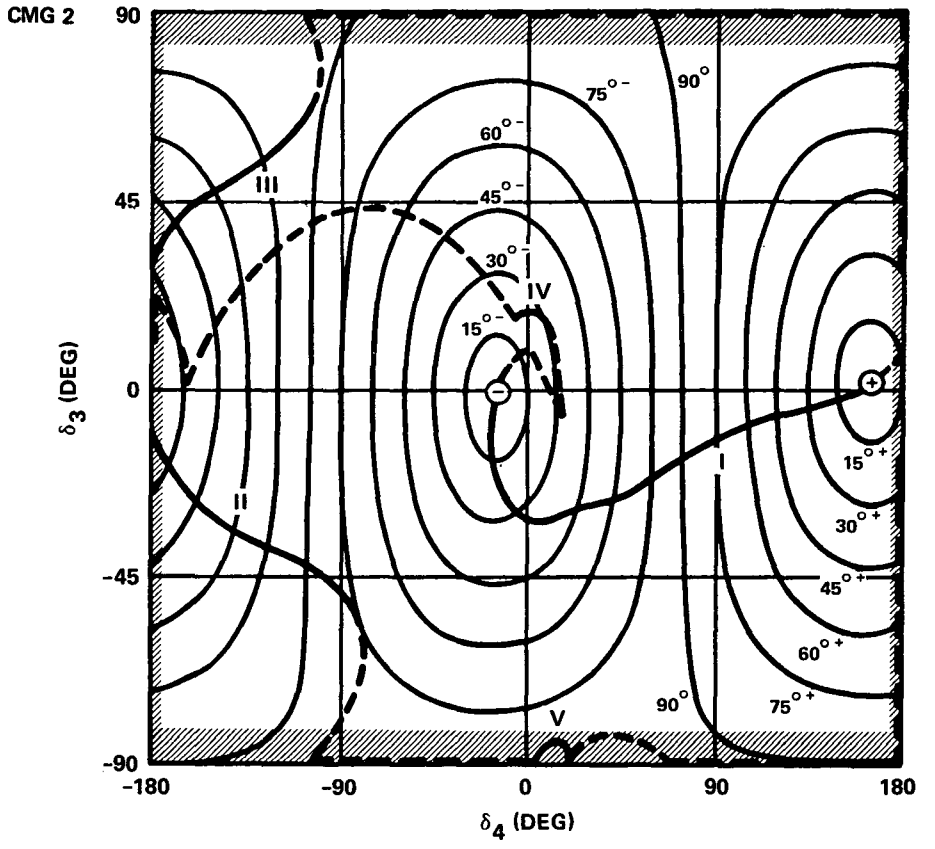

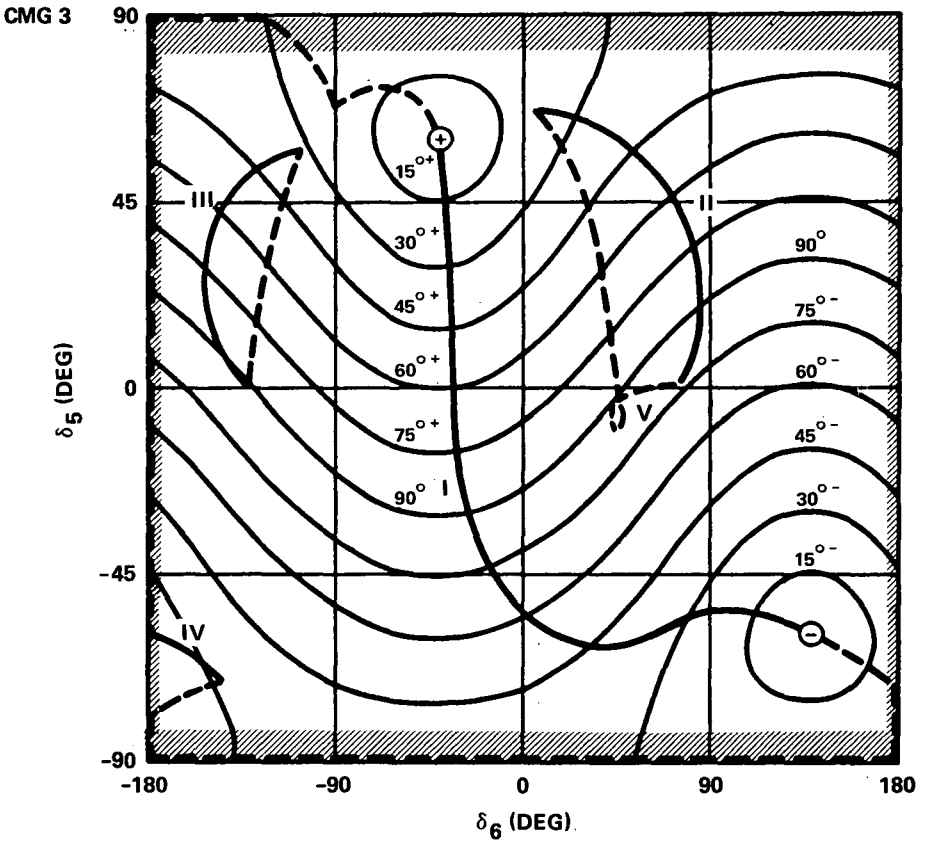

FIGURE 16 EQUILIBRIUM LOCI FOR CMG s 2 & 3 FOR $\underline{h} = \pm(0, -.866, .5)^T$

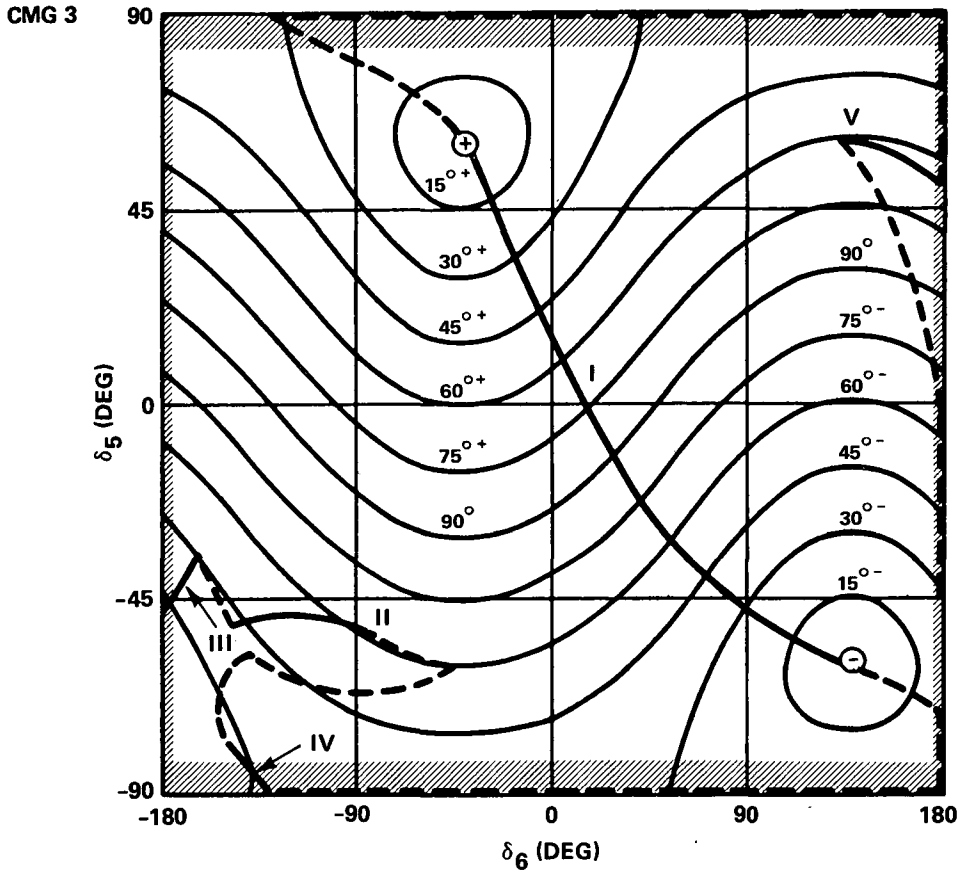

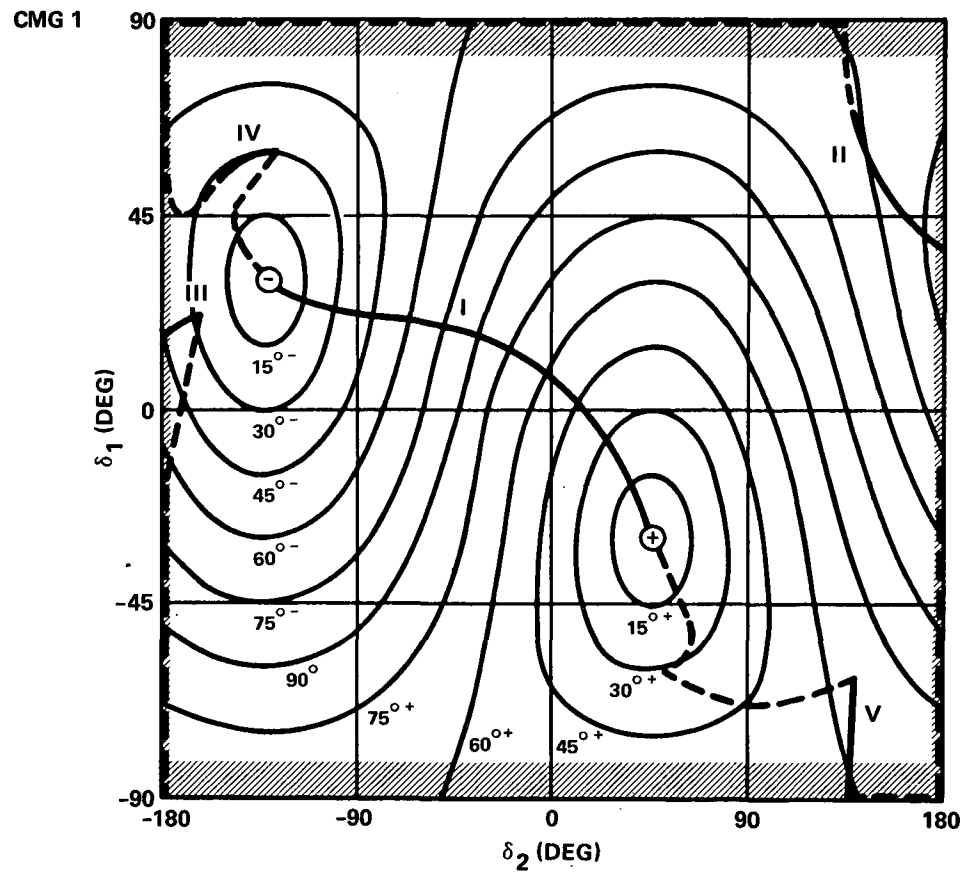

FIGURE 17 EQUILIBRIUM LOCI FOR CMG s 3 & 1 FOR $\underline{h} = \pm(0, -.866, .5)^T$

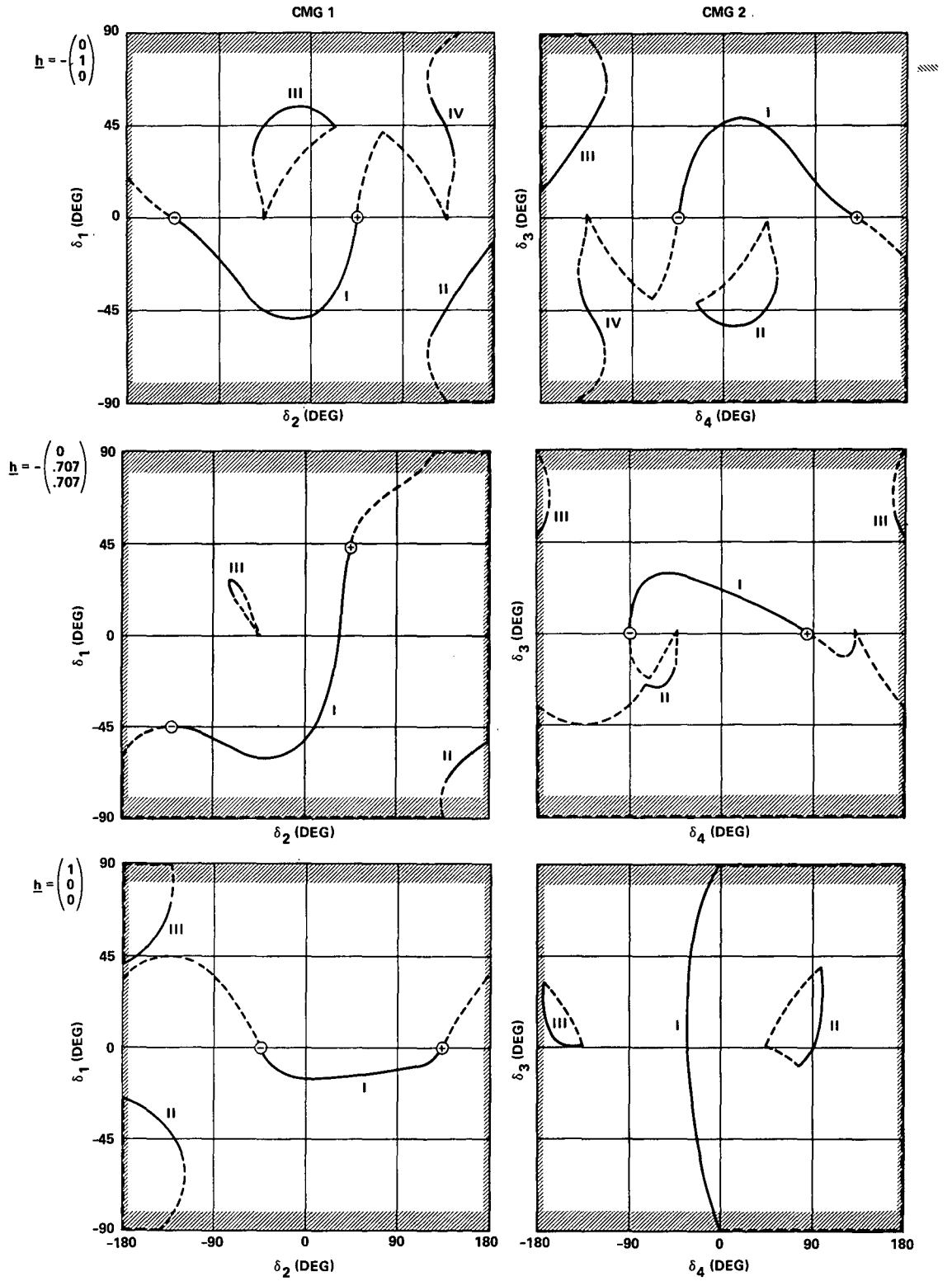

FIGURE 18 EQUILIBRIUM LOCI FOR CMG s 1 & 2 FOR VARIOUS $\underline{h}$

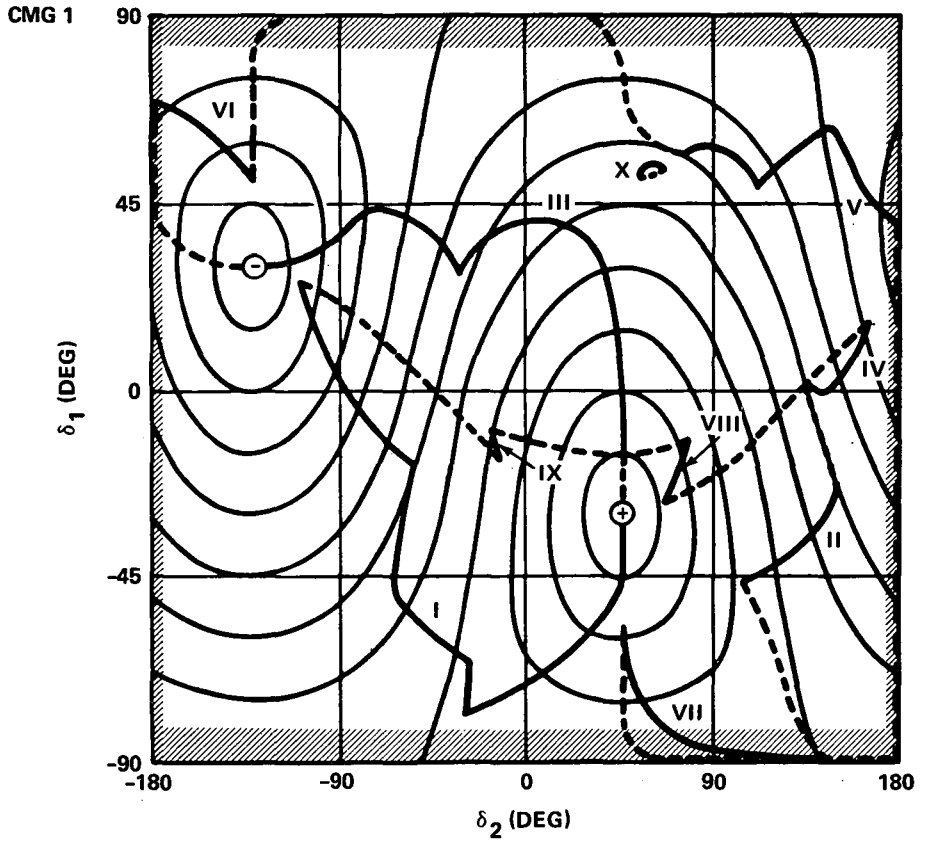

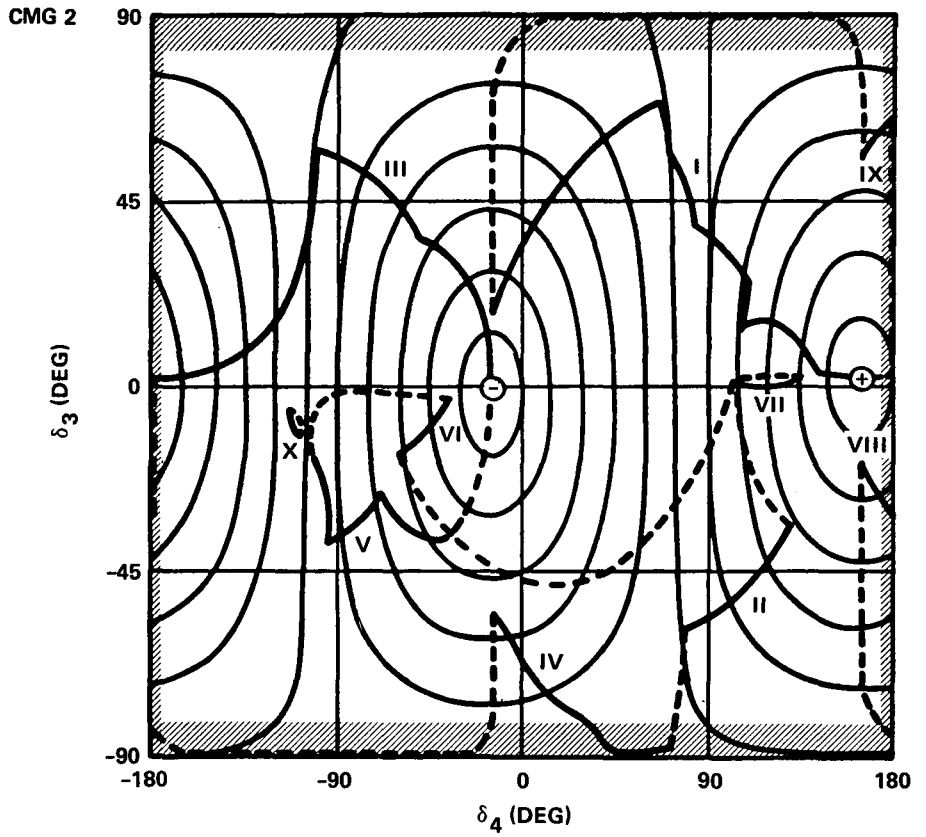

FIGURE 19 EQUILIBRIUM LOCI FOR CMG s 1 & 2 FOR $\underline{h} = \pm (0, -.866, .5)^T$ WITH SL LIMITING (SL = .04)

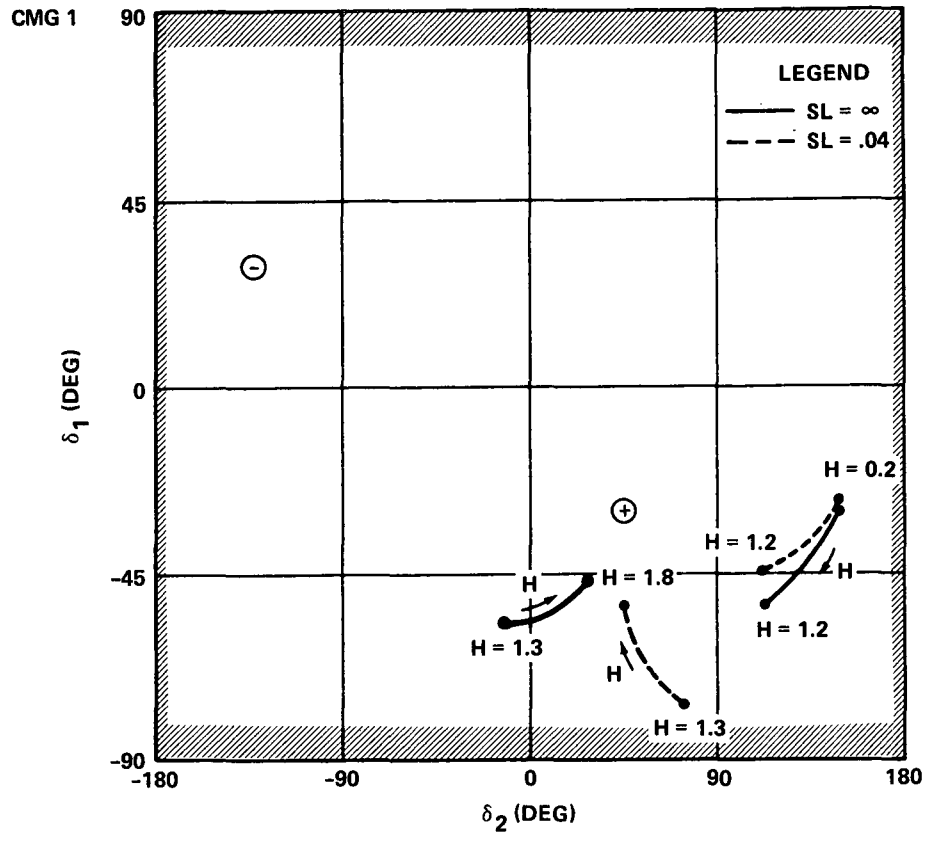

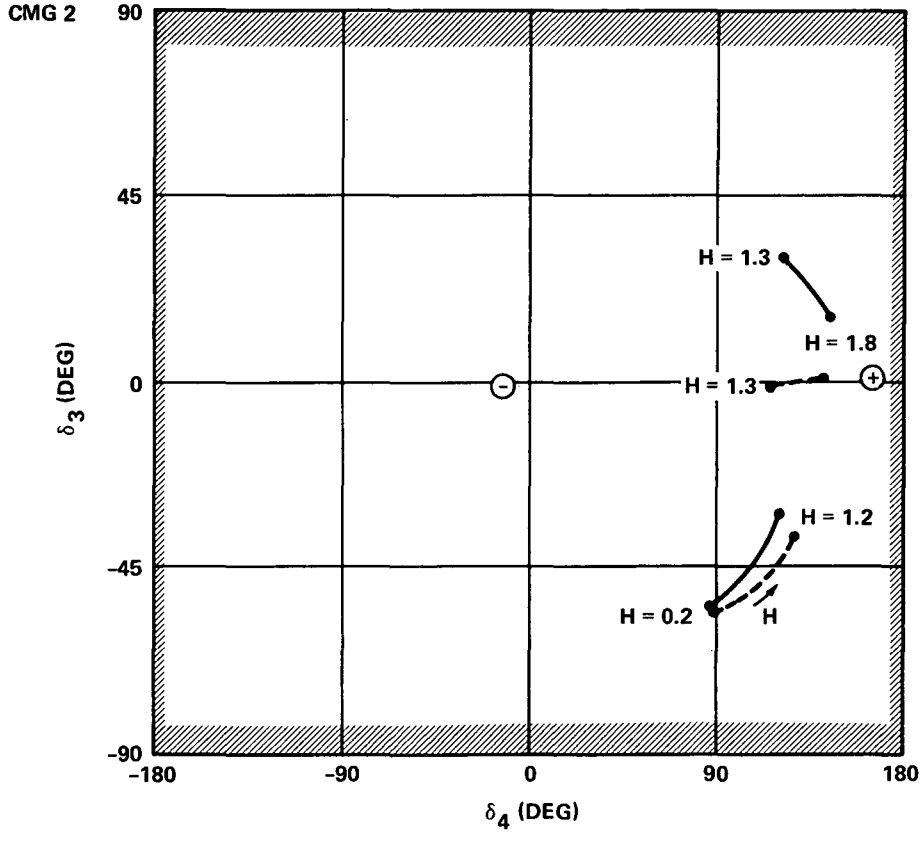

FIGURE 20 EQUILIBRIA ACQUIRED FOR CMG's 1 & 2 AFTER CAGING TO $\underline{h} = (0, -.866, .5)^T$ AND $0.2 \leq H \leq 1.8$ WITH AND WITHOUT SL LIMITING

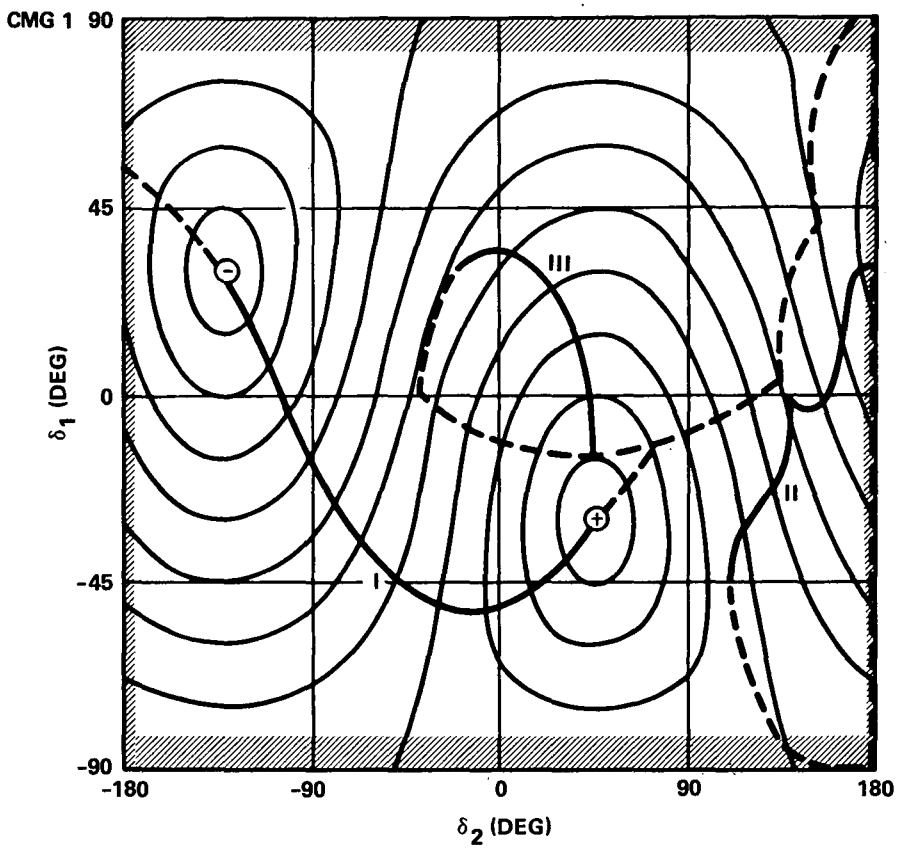

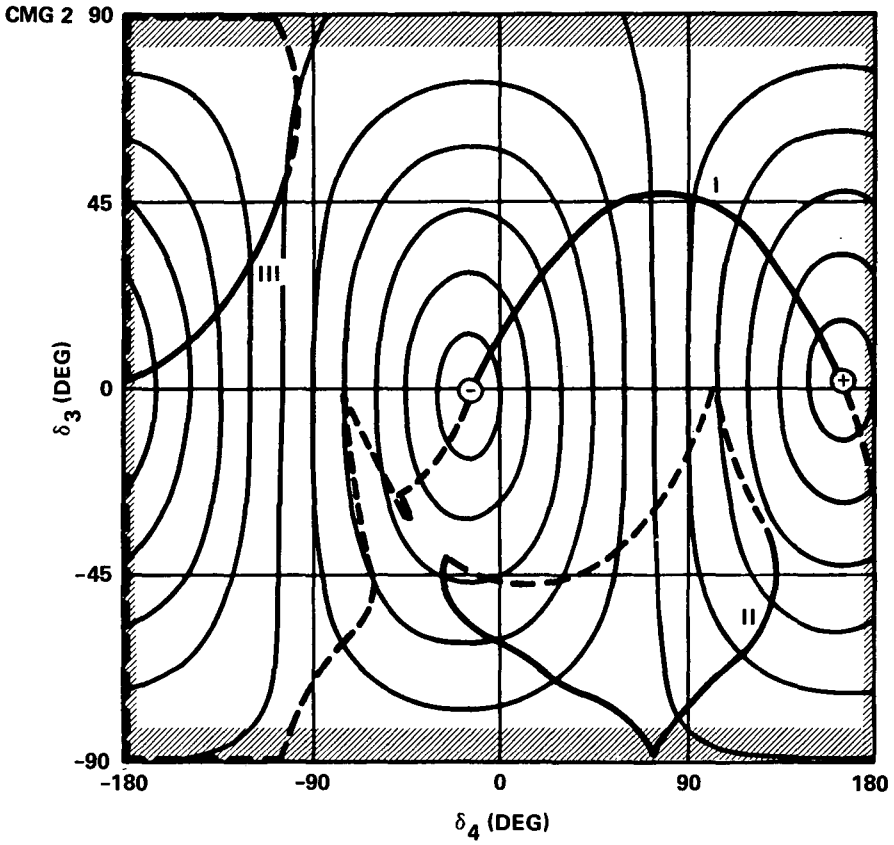

FIGURE 21 EQUILIBRIUM LOCI FOR CMG s 1 & 2 FOR $\underline{h} = \pm(0, -.866, .5)^T$ AND $\underline{\delta}_N \neq \underline{0}$

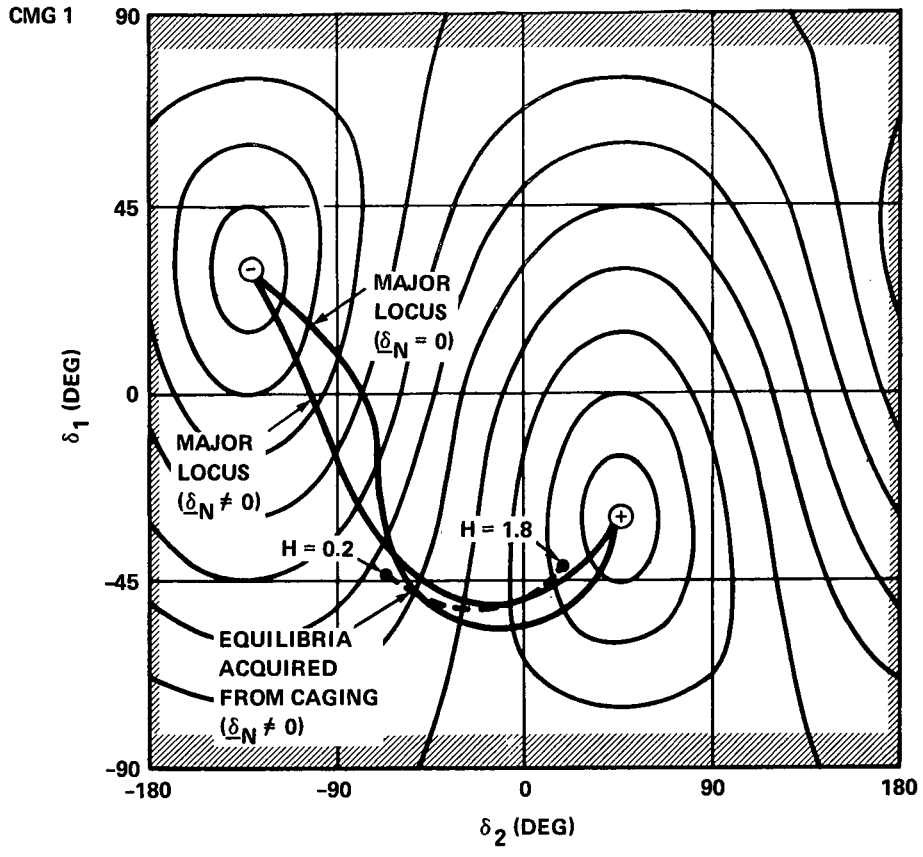

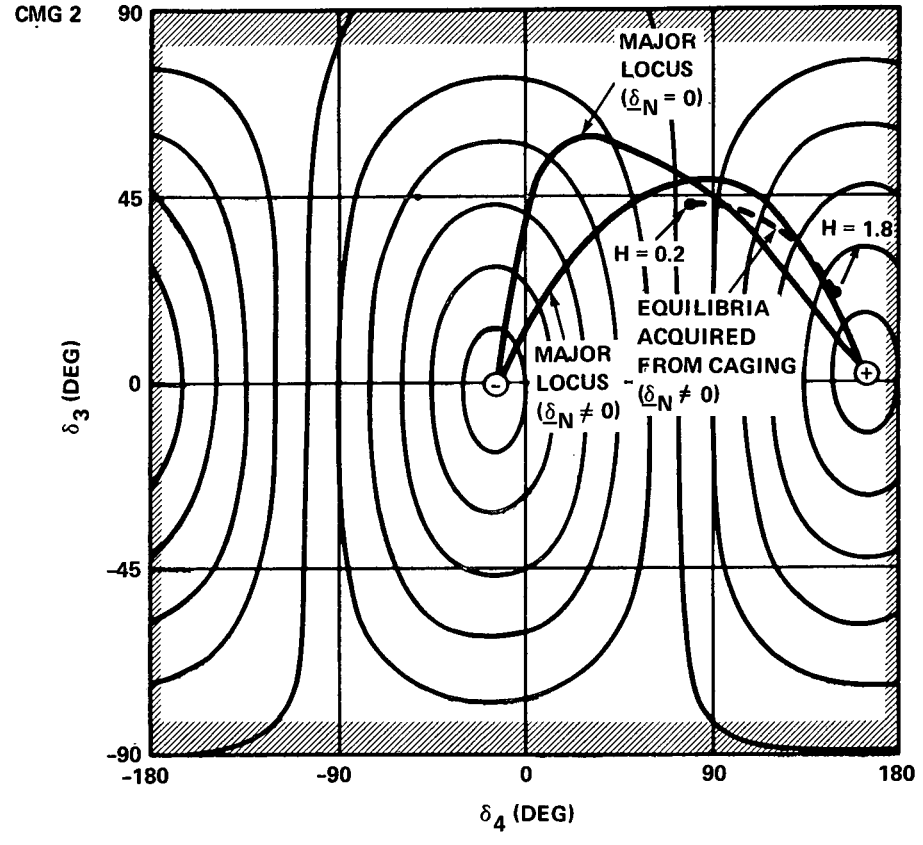

FIGURE 22 MAJOR EQUILIBRIUM LOCI FOR CMG s 1 & 2 AND $\underline{\delta}_E$ ACQUIRED FROM CAGING TO $\underline{h} = (0, -.866, .5)^T$ AND $0.2 \leq H \leq 1.8$ FOR $\underline{\delta}_N = \underline{0}$ AND $\underline{\delta}_N \neq \underline{0}$

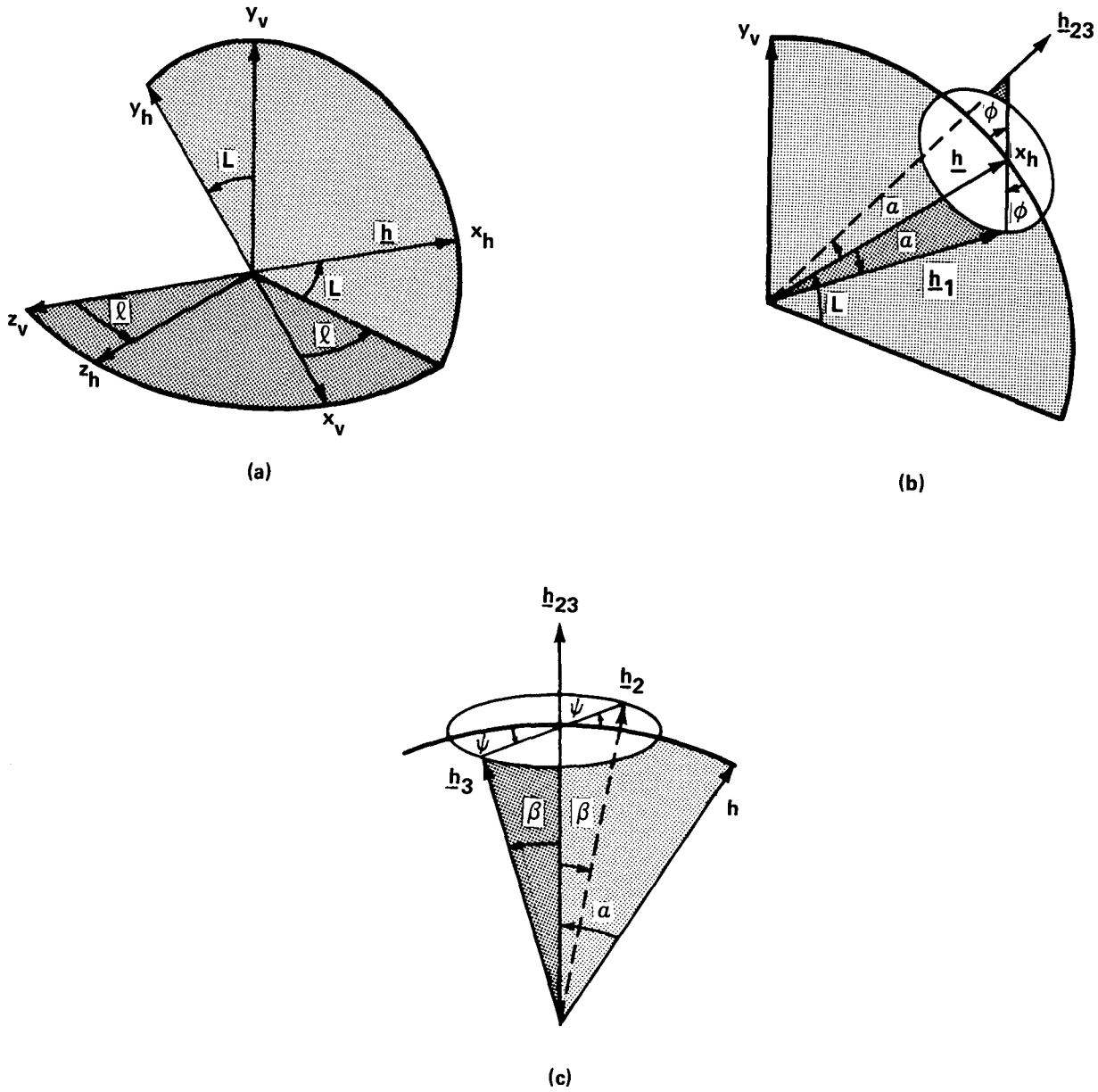

FIGURE B-1 - ORIENTATION OF GYRO MOMENTUM VECTORS

(a)

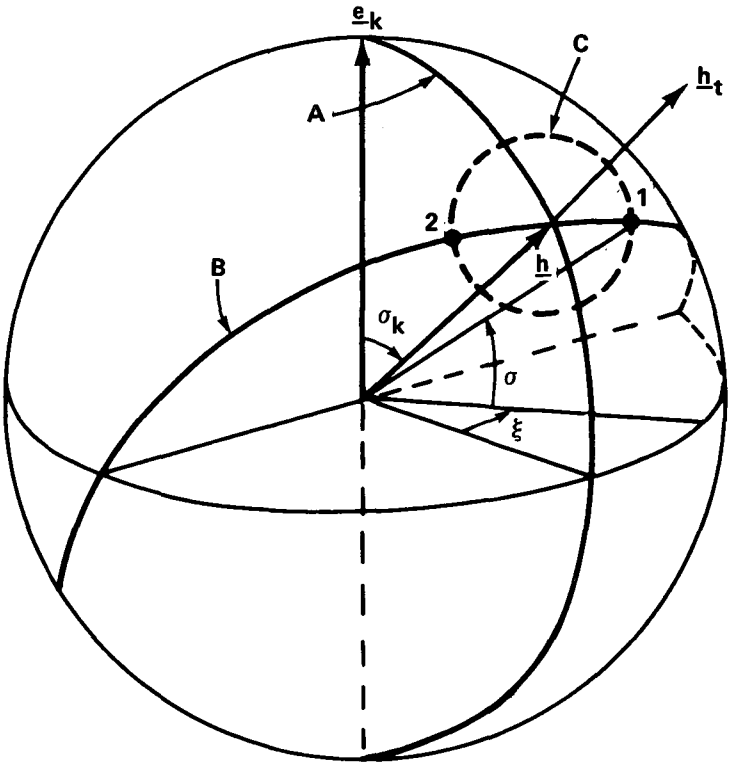

(b)

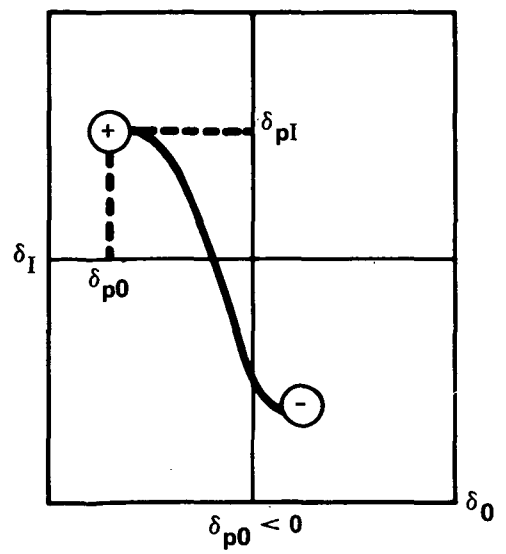

(c)

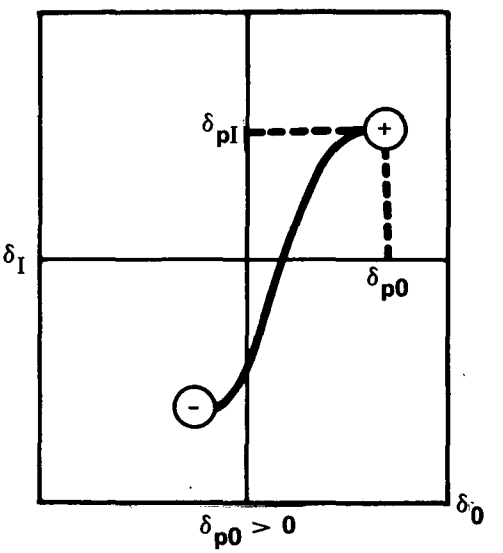

FIGURE (C-1) GEOMETRY FOR DYNAMIC ORIGIN LOCUS AND TYPICAL TRAJECTORIES IN GIMBAL ANGLE SPACE

References

1. "Apollo Telescope Mount Digital Computer (ATMDC) Program Definition Document (PDD)", Part I, Phase 1A Program, IBM (Huntsville) Report No. 70-207-0002, October 15, 1971.

2. J. Kranton, "Analytical Development of the Skylab CMG Rotation Law", Bellcomm Memorandum for File, B70 06082, June 29, 1970.

3. W. Hahn, "Stability of Motion" (book), Springer Verlag, New York, N.U., 1967, pp. 102-104.

4. R. W. Grutzner, "User's Guide for SACSIM - Skylab Attitude Control Simulation", Bellcomm Memorandum for File B72 03006, March 8, 1972.

5. W. Levidow, "Skylab CMG Gimbal Angle Behavior and Attitude Control Performance," Bellcomm Memorandum for File B72 03015, March 31, 1972.

6. S. C. Chu and J. Kranton, "Design of Control Laws for Control Moment Gyroscopes with Application to Skylab", Bellcomm Technical Memorandum TM-71-1022-4, September 3, 1971.